

Figure #	Figure title One sentence only	Filename This should be the name the file is saved as when it is uploaded to our system. Please include the file extension. i.e.: <i>Smith_ED_Fig1.jpg</i>	Figure Legend If you are citing a reference for the first time in these legends, please include all new references in the Online Methods References section, and carry on the numbering from the main References section of the paper.
Extended Data Fig. 1	Pre-existing innate type-2 inflammation promotes lung metastasis formation.	Schuijs_M_FigS1.jpg	<p>a, WT mice were treated as in (<i>Fig. 1a</i>) and tumor burden was assessed by histological staining for Ki67⁺ tumor foci and quantification of tumor area over total lung area by automated image analysis (n = 10). b, <i>Il33^{cit/+}</i> reporter mice were treated intranasally with PBS or IL-33 on days 0 and 1, and citrine⁺ lung cells were assessed on day 3. c, WT mice were treated intranasally with IL-33 on days 0 and 1 (or PBS injection for day 0), followed by quantification of total lung eosinophils by flow cytometry (<i>see Extended Data Fig 4a for gating strategy</i>) at the indicated time-points (n = 3). d, WT mice were treated as indicated, followed by visual quantification of lung metastases on day 28 (n = 9). e, WT mice were treated as indicated, followed by visual quantification of lung metastases on day 21 (n = 6). f, WT mice were treated intranasally with LPS, CpG or PBS on days 0 and 1, followed by intravenous transfer of B16.F10 cells on day 7, and sacrifice on day 21, followed by visual quantification of lung metastases (n = 10). g, 4T1 (n = 10) or 4T1-T (n = 13,14,10) breast cancer cells were implanted</p>

			<p>in the mammary fat pad (see <i>Methods</i>), primary tumors were dissected and weighed. h, B6.MMTV-PyMT mice were randomized, treated intranasally with PBS, IL-33, or Asp (from week 12 to 20, see <i>Methods</i>), followed by measurement of total primary breast tumor(s) weight at 20 weeks of age (n = 10,10,11). i, Representative flow cytometry gating strategy of lung lymphocytes and innate lymphocyte populations from WT mice treated with PBS or IL-33 on day 0 and 1, followed by sacrifice on day 3 description of gated cells is listed above the dot plot, cell exclusion performed by Boolean-gating. j, WT mice were treated as in (c), followed by quantification of total lung ILC2 (Live CD45⁺CD3⁻B220⁻NK1.1⁻Lineage⁻CD127⁺RORγt⁻GATA3⁺) at the indicated time points (n = 3). k, WT and <i>Il33</i>^{-/-} mice were treated with PBS or Asp on day 0 and 1, followed by quantification of total lung eosinophils at day 3 (n = 10,10,5,10).</p> <p>Bar graphs indicate mean (±SEM) and show combined data of two (d-f, k, g) or three (a, h), or representative of three independent experiments (b, c, i, j c). Statistical analyses were calculated using one-way ANOVA with **** = p ≤ 0.0001.</p>
Extended Data Fig. 2	IL-33 influences lung NK cells.	Schuijs_M_FigS2.jpg	a , WT mice were treated as indicated, followed by visual quantification of lung metastases on day 21.

		<p>b, WT mice were treated with anti-IFNγ or control mAb similar to (a); Tumor burden was assessed on day 21 by visual quantification of lung metastases (n = 10). c, Mice were treated intranasally with PBS or IL-33 on days 0 and 1, followed by quantification of total lung NK cells by flow cytometry on day 3 (n = 3). d, WT mice were treated as in (c), followed by flow cytometric detection of Ki-67⁺ lung NK cells and ILC2 (n =5). e, Representative flow cytometry gating strategy of lung NK cells and T lymphocytes from WT mice treated with PBS or IL-33 on day 0 and 1, followed by sacrifice on day 3. f,g, WT mice were treated as in (c), followed by quantification of IFNγ⁺ NK cells (Live CD45⁺NK1.1^{+/low}CD49b⁺) after 3hr stimulation of total lung cells with plate bound anti-NK1.1 (f) (n = 3); or PI (g) (n = 3). h, Total WT mouse lung cells were stimulated for 3hrs <i>ex vivo</i> with a combination of IL-12 and IL-18, followed by quantification of IFNγ⁺ positive NK cells (n = 10). i, WT mice were treated as in (c) and cardiac WAT NK cell were analyzed for intracellular IFNγ (n = 9,6) and GzmB (n = 9,6) after 3hr stimulation with PI. j, Lung CD4 and CD8 T cells from PBS or IL-33 treated WT mice were analyzed for intracellular IFNγ after 3hr stimulation with PI or anti-NK1.1 (representative gating shown in (e)). k, WT mice were treated as in (c), followed by lung NK cells purification and co-cultured with CFSE labelled whole lung</p>
--	--	--

			<p>homogenates from PBS or IL-33 treated WT mice (12h), followed by 3hr PI stimulation and detection of GzmB positive NK cells; grey bars indicate CFSE-labelled NK cells present in whole lung homogenates (n = 6,11,10,11,2,8 biologically independent samples). l-m, WT mice housed at the MRC ARES facility were treated as in (c), followed by quantification of percent of IFNγ⁺ NK cells (after 3hrs of PI) (l) (n =5), or treated as in Fig. 1a (50K B16.F10) followed by visual quantification of lung metastases (m) (n = 5).</p> <p>Bar graphs indicate mean (\pmSEM) and show combined data of two (b, i) or three (h, k) independent experiments. (e, j) show representative flow cytometry plots of three independent experiments, whereas (c, d, f, g, l, and m) show a representative bar graph of two independent experiments. Statistical analyses were calculated using one-way ANOVA or unpaired two-tailed Student's t-test (c, f-i, l, m) **** = p \leq 0.0001.</p>
Extended Data Fig. 3	ILC2 suppress NK cells via an indirect innate immune mechanism.	Schuijs_M_FigS3.jpg	<p>a, <i>Il7ra</i>^{Cre/+} or <i>Il7ra</i>^{Cre/+}<i>Rora</i>^{fl/fl} mice were treated with PBS or Asp on day 0 and 1, followed by quantification of IFNγ⁺ lung NK cells on day 3 (n = 12,13,11,12). b,c, WT mice were treated as in (a), followed by purification of lung ILC2 (flow cytometry) and lung NK cells (magnetic bead, see Methods) on</p>

		<p>day 3. Lung NK were cultured alone or with ILC2 and analyzed for intracellular IFNγ and GzmB (c) (n = 8). d, WT mice were treated as in (e) with PBS or IL-33 and A2AR antagonist or DMSO followed by quantification of IFNγ⁺ lung NK cells on day 3 (n = 6,7,6). e, WT mice were treated as indicated, followed by quantification of GzmB⁺ lung NK cells (n = 3, representative gating on right). f, WT and Foxp3^{DTR} mice were treated with PBS or IL-33 and DTx, followed by quantification of percent IFNγ⁺ lung NK cells on day 3 (n = 3,3,4,5). g, WT and <i>Rag2</i>^{-/-} mice were treated with PBS or IL-33 on days 0 and 1, and given adoptive transfer of LL/2 cells (i.v.) on day 7. Tumor burden was assessed on day 21 by visual quantification of lung metastases (n = 10,8,8,10). h, WT, <i>Rag2</i>^{-/-} and <i>Rag2</i>^{-/-} <i>Il7ra</i>^{Cre/+} <i>Rora</i>^{fl/fl} mice were treated with PBS or IL-33 on day 0 and 1, followed by flow cytometry analysis for the indicated lung lymphoid cells on day 3 (n = 5).</p> <p>Bar graphs indicate mean (\pmSEM) and show combined data of two (c, d, and g) or three (a) independent experiments. (e, f, and h) shows a representative bar graph of two independent experiments. Statistical analyses were calculated using one-way ANOVA with ns = not significant, and **** = p \leq 0.0001.</p>
--	--	--

Extended Data Fig. 4	Myeloid cell profiling after IL-33 administration and correlation with NK cell function.	Schuijs_M_FigS4.jpg	<p>a,b, WT mice were treated with PBS or IL-33 on day 0 and 1, followed by (a) flow cytometry analysis and (b) quantification for the indicated lung myeloid cells on day 3 (n = 6). c, Representative flow cytometry plot of eosinophils from mice injected and gated as in (a) assessed for expression of Ly-6G (left) Ly-6C (right). d, The correlation between percent IFNγ⁺ NK cells and total numbers of the indicated myeloid cells in the lung of PBS or IL-33 injected WT mice (day 0 and 1, sacrificed on day 3) was analyzed on pooled results (n=125).</p> <p>Bar graphs indicate mean (\pmSEM) and show representative data from three independent experiments (a, b, and c) and (d) representing Pearson r.</p>
Extended Data Fig. 5	IL-33-mediated suppression of NK cells is not dependent on neutrophils or alveolar macrophages.	Schuijs_M_FigS5.jpg	<p>a-e, WT mice were treated with PBS or IL-33 on day 0 and 1, and the indicated mAb (or clodronate liposomes, C.L.) on day -1 and 1 followed by quantification of percent IFNγ⁺ or GzmB⁺ lung NK cells (after PI stimulation) and quantification for the indicated lung myeloid cells on day 3 (a; GzmB n = 10,9,9,10, and depicted myeloid cells n = 15,14,14,15, b; n = 8,8,8,9, c; n = 7, d,e, n = 6).</p> <p>Bar graphs indicate mean (\pmSEM) and show</p>

			combined data of two (b-e) or three (a) independent experiments. Statistical analyses were calculated using one-way ANOVA with ns = not significant, and **** = $p \leq 0.0001$
Extended Data Fig. 6	IL-5 and eosinophils mediate IL-33-driven suppression of NK cells.	Schuijs_M_FigS6.jpg	<p>a, WT mice were treated with PBS or IL-33 on day 0 and 1, followed by quantification of IL-5⁺ ILC2 (CD45⁺B220⁻Lineage⁻), or CD45⁺B220⁻lineage⁺ cells in the lungs on day 3 (n = 5); the identity of IL-5⁺ ILC2 was further confirmed by ICOS expression.</p> <p>b-d, WT mice were treated with PBS or IL-33 on day 0 and 1, and anti-IL-5 or control on day -6, -3 and -1 followed by quantification of the total numbers of the indicated myeloid cells in the lung (c) (n = 10), and the percent IFNγ⁺ and GzmB⁺ lung NK cells (after anti-NK1.1 stimulation) on day 3 (d) (n = 5).</p> <p>e, WT mice were treated intranasally with PBS or the indicated cytokines on day 0 and 1, followed by quantification of percent IFNγ⁺ NK cells (after PI stimulation), or lung eosinophil numbers on day 3 (n = 3).</p> <p>f, Mice of the indicated genotypes were treated intranasally Asp or PBS on days 0 and 1, followed by intravenous transfer of B16.F10 cells on day 7 and subsequent determination of lung metastases-related mortality by Kaplan-Meier survival curve (n = 15,14,15,9).</p> <p>g, Purified WT mouse lung NK cells were cultured alone or with <i>ex vivo</i> bone marrow derived eosinophils at the indicated ratios for 18</p>

			<p>hours, followed by a 3hr re-stimulation with PI and quantification of IFNγ⁺ and GzmB⁺ NK cells by flow cytometry (n = 6,6,9).</p> <p>Bar graphs indicate mean (\pmSEM) of combined data of two (c, g) or three (f) independent experiments. (d and e) show representative data of three independently performed experiments and (a) depicts representative flow cytometry plots. Statistical analyses were calculated using one-way ANOVA or Log-rank (Mantel-Cox) test (f) with **** = $p \leq 0.0001$.</p>
Extended Data Fig. 7	Single-cell and bulk-RNA-seq of naive and IL-33-inflamed lung NK cells.	Schuijs_M_FigS7.jpg	<p>a, Mice were treated with PBS or IL-33 on day 0 and 1, followed by FACS purification of lung NK cells at the indicated time-points for either scRNA-seq or bulk-RNA-seq analysis. b, Post FACS purity was assessed for all sorts. c, Clusters from (Fig. 4a) were annotated based on their gene expression patterns. Heatmap of genes significantly (FDR < 0.05) upregulated or downregulated in one cluster versus all others. Where more than 15 genes were significantly differentially expressed, only the 15 with the greatest average log-fold changes in each direction were included. Blue-to-yellow color gradient indicates log₂ (normalized gene expression). d, scRNA-seq expression of <i>Cd27</i> and <i>Itgam</i> (encoding CD11b) separated by cluster.</p>

		<p>Specific clusters were annotated as follows (where individual genes were significantly upregulated in one cluster compared to all others, the 5 with greatest average log-fold-change are listed as marker genes): Cluster 2: signaling/inflammatory-chemokine-expressing NK cells (<i>Pim1</i>, <i>Nfkbia</i>, <i>Gadd45b</i>, <i>Ccl4</i>, <i>Icam1</i>); Cluster 3: (<i>Kcnj8</i>, <i>Ly6c2</i>); Cluster 4: (<i>Hsp90ab1</i>, <i>Hspe1</i>, <i>Nme1</i>, <i>Ptma</i>, <i>Rps2</i>); Cluster 6: (<i>Ccl5</i>, <i>Cma1</i>, <i>Klrg1</i>, <i>Itm2b</i>); Cluster 7: immature NK cells (<i>Ctla2a</i>, <i>Emb</i>, <i>Ccr2</i>, <i>Rps15a</i>, <i>Rpl10a</i>). Cluster 2 was most similar to the previously identified splenic murine NK cell cluster 3, and Cluster 7 was most similar to the previously identified splenic and blood murine NK cell cluster 2 as identified by Crinier <i>et al.</i>³². e, Results of a differential abundance analysis comparing the abundance of cells in each cluster after IL-33 versus PBS treatment. P-values were calculated using empirical Bayes quasi-likelihood F-tests in a negative binomial GLM (as described in <i>Methods</i>). f,g, Expression of NK cell consensus³², effector, and both activating and inhibitory receptor transcripts from bulk-RNA-seq analysis of sorted lung NK cells. Data are represented as a heatmap of log₂-transformed normalized read counts of individual genes, grouped by category (f), or z-scaled expression values for genes within the 4 gene lists. Each point represents the expression value obtained</p>
--	--	---

			<p>by one replicate for a given gene at a given time point (g). Box plots represent mean (black line), first and third quartiles (box) and range within 1.5 times the interquartile range from the box (whiskers). Violin plots represent median (black line), interquartile ranges (box) and a kernel density plot.</p>
Extended Data Fig. 8	IL-33 increases glucose flux in the lung environment via ILC2 and IL-5.	Schuijs_M_FigS8.jpg	<p>a, BALB/c mice were treated intranasally with IL-33 or PBS on days 0 and 1, and anti-IL-5 or control antibody (i.p.) on day -6, -3, and 0 and sacrificed on day 3. Lung homogenates were cultured for 18 hours and glucose (Glu) and lactate (Lac) concentrations were measured in the supernatant by NMR analysis (n = 10,9,9). b, Spatial resolving glycolytic activity in lung by MSI. WT or <i>Ii7ra</i>^{Cre/+}<i>Rora</i>^{fl/fl} (KO) mice were dosed with PBS or IL-33 on day 0 and 1, and sacrificed on day 3 and infused or not with [U-¹³C] glucose (as described in <i>Methods</i>). (Right to left) H&E stained lungs and post DESI-MSI molecular images of lactate, [U-¹³C] lactate, glucose, [U-¹³C] glucose, normal and [U-¹³C] lactate to glucose ratio (pixel per pixel). Intensity scale is fixed for each molecular species independently, and monochromatic lighter colors correspond to higher relative abundance. c, d, Bar graphs indicate mean relative abundances of [U-¹³C] glucose or [U-¹³C] lactate (c) (n = 4), or the ratio of [U-¹²C] lactate over glucose (d) (n = 4). e, BALB/c were treated intranasally with Asp or PBS on days 0</p>

			<p>and 1, and anti-IL-5 or control antibody (i.p.) on day -6, -3, 0 and 3, followed by injected with 4T1-T breast cancer cells in the mammary fat pad on day 7, and sacrifice on day 21. f, Tumor burden of mice treated as in (e) with 4T1-T cells was quantified by visual examination and primary tumor weight was recorded (n = 9,10,9). g, Graphical abstract.</p> <p>Bar graphs indicate mean (\pmSEM) of combined data of two (a, c, d, and f) independent experiments. (b) depicts representative MSI images of two independent experiments. Statistical analyses were calculated using one-way ANOVA with **** = $p \leq 0.0001$.</p>
--	--	--	--

1

Item	Present?	Filename	A brief, numerical description of file contents. i.e.: <i>Supplementary Figures 1-4, Supplementary Discussion, and Supplementary Tables 1-4.</i>
Supplementary Information	No	This should be the name the file is saved as when it is uploaded to our system, and should include the file extension. The extension must be .pdf	
Reporting Summary	Yes	Reporting Summary (Schuijs MJ et al.).pdf	
Peer Review Information	Yes	OFFICE USE ONLY	

2

3

4

5
6
7
8
9
10
11
12
13
14
15
16
17
18
19
20
21
22
23
24
25
26
27
28
29
30
31
32

ILC2-driven innate immune checkpoint mechanism antagonizes NK cell anti-metastatic function in the lung

Martijn J. Schuijs¹, Shaun Png¹, Arianne C. Richard^{1,2}, Anastasia Tsyben^{1,3}, Gregory Hamm⁴, Julie Stockis¹, Celine Garcia¹, Silvain Pinaud¹, Ashley Nicholls¹, Xavier Romero Ros⁵, Jing Su¹, Matthew D. Eldridge¹, Angela Riedel⁶, Eva M. Serrao¹, Hans-Reimer Rodewald⁷, Matthias Mack⁸, Jacqueline D. Shields⁶, E. Suzanne Cohen⁵, Andrew N.J. McKenzie⁹, Richard J.A. Goodwin⁴, Kevin M. Brindle^{1,10}, John C. Marioni^{1,11,12} & Timotheus Y.F. Halim^{1,13}

Institutions:

- ¹ University of Cambridge, CRUK Cambridge Institute, Cambridge, UK
- ² University of Cambridge, Cambridge Institute for Medical Research, Cambridge, UK
- ³ Addenbrooke's Hospital, Cambridge University Hospitals NHS Foundation Trust, Cambridge, UK
- ⁴ Imaging and Data Analytics, Clinical Pharmacology and Safety Sciences, BioPharmaceuticals R&D, AstraZeneca, Cambridge, UK
- ⁵ Bioscience Asthma, Research and Early Development, Respiratory & Immunology, BioPharmaceuticals R&D, AstraZeneca, Cambridge, UK
- ⁶ MRC Cancer Unit, University of Cambridge, Cambridge, UK
- ⁷ Division of Cellular Immunology, German Cancer Research Center, Heidelberg, Germany
- ⁸ University Hospital of Regensburg, Department of Internal Medicine, Regensburg, Germany

33 ⁹ MRC Laboratory of Molecular Biology, Cambridge, UK

34 ¹⁰ University of Cambridge, Department of Biochemistry, Cambridge, UK

35 ¹¹ EMBL-European Bioinformatics Institute, Wellcome Genome Campus, Cambridge, UK

36 ¹² Wellcome Sanger Institute, Wellcome Genome Campus, Cambridge, UK

37

38

39

40 Corresponding author:

41 ¹³ Tim.Halim@cruk.cam.ac.uk

42

43

44

45 **Abstract**

46

47 **Metastasis constitutes the primary cause of cancer-related deaths, with the lung being a commonly affected organ. Here we found**
48 **that activation of lung-resident group 2 innate lymphoid cells (ILC2) orchestrated suppression of Natural Killer (NK) cell-mediated**
49 **innate anti-tumor immunity, leading to increased lung metastases and mortality. Using multiple models of lung metastasis, we show**
50 **that IL-33-dependent ILC2-activation in the lung is centrally involved in promoting tumor burden. ILC2-driven innate type-2**
51 **inflammation is accompanied by profound local suppression of interferon- γ production and cytotoxic function of lung NK cells. ILC2-**
52 **dependent suppression of NK cells is elaborated via an innate regulatory mechanism, reliant on IL-5-induced lung eosinophilia,**
53 **ultimately limiting the metabolic fitness of NK cells. Therapeutic targeting of IL-33 or IL-5 reversed NK cell suppression, and**
54 **alleviated cancer burden. Thus, we reveal an important function of IL-33 and ILC2 in promoting tumor metastasis via their capacity to**
55 **suppress innate type-1 immunity.**

56

57 Many cancers spread to the lung, with grave consequences for patient survival¹. For the formation of lung metastases, circulating tumor cells
58 (CTC) must extravasate into the tissue interstitium and evade tissue-resident immune cells. Lung Natural Killer (NK) cells are the innate
59 counterpart to cytotoxic CD8⁺ T cells and comprise approximately 10-20% of all lung-resident lymphocytes in humans and mice. NK cells are
60 critical for antigen-independent recognition and elimination of infiltrating CTC, as demonstrated by overwhelming metastatic burden in their
61 absence or impairment².

62

63 Group 2 innate lymphoid cells (ILC2) are the innate counterpart to adaptive CD4⁺ T_H2 cells, and like NK cells, comprise a tissue-resident
64 population in the naive lung³. Lung ILC2 are activated by the alarmin interleukin (IL)-33 which is released from various immune and non-
65 immune cell-types upon lung injury, infection, or allergen exposure⁴. ILC2 mediate innate and adaptive type-2 inflammation through rapid
66 release of effector cytokines such as IL-5 and IL-13, and expression of costimulatory ligands that influence T_H2 cells⁴. ILC2 also closely interact
67 with regulatory T cells (T_{reg}) cells, indicating a potential contribution to immune-suppressive functions^{5, 6}. Relatedly, several groups describe
68 distinct regulatory ILC that can counter type-1 immunity^{7, 8}, or ILC2-specific expression of immune-suppressive molecules⁹. Nevertheless, it
69 remains unclear if the physiological role of ILC2 extends beyond regulating type-2 immunity.

70

71 Although type-2 inflammation is largely associated with tumor progression, via type-2 cytokine-mediated polarisation of alternatively activated
72 macrophages and myeloid derived suppressor cells, IL-33 has both pro- and anti-tumor functions in primary solid, and haematological
73 malignancies¹⁰. Similarly, opposing functions for ILC2 are reported in the primary tumor environment^{11, 12, 13}. Nevertheless, type-2 inflammation
74 is associated with metastasis formation^{14, 15}. Given the central role of lung ILC2 in directing innate and adaptive type-2 immunity⁴, we
75 hypothesized that ILC2 activation in the pre-metastatic niche can influence the formation of lung metastases.

76

77 Here we demonstrate that pre-existing type-2 airway inflammation greatly increases metastatic seeding of the lung in an IL-33- and ILC2-
78 dependent pathway. In addition to orchestrating type-2 inflammation, ILC2 also profoundly suppress NK cell-driven anti-tumor immunity
79 independent of the adaptive immune system. Mechanistically, ILC2 mediate their immunosuppressive effect via recruitment and activation of
80 eosinophils in an IL-5 dependent manner. Eosinophils, but not ILC2, are able to directly suppress NK cell function by modulating the metabolic

81 environment of the inflamed niche. Therapeutic intervention reverses lung NK cell metabolic restraint, effector molecule production and anti-
82 tumor function. As such, we demonstrate the important function of ILC2 in cancer dissemination to the lung, and further reveal a novel immune-
83 regulatory collaboration between ILC2 and eosinophils that antagonizes innate type-1 immunity.

84

85 **Results**

86

87 **IL-33-driven activation of ILC2 is critical for promoting lung metastases**

88

89 To assess the effect of airway innate type-2 inflammation on lung metastasis formation, we employed a model of IL-33 or *Aspergillus* protease
90 allergen (Asp) induced airway inflammation prior to adoptive transfer of metastatic B16.F10 melanoma cells (Fig. 1a). We noted a significant
91 increase in metastatic burden by day 21, and increased mortality in both IL-33 or Asp conditioned mice (Fig. 1b, c, d, Extended Data Fig. 1a).
92 Protease allergens can activate lung-resident ILC2 via IL-33-release¹⁶, which is produced primarily by EpCAM⁺ epithelial cells (Extended Data
93 Fig. 1b). Resolution of acute type-2 inflammation after 14 days, as measured by lung eosinophilia, diminished the pro-metastatic effect of IL-33
94 (Extended Data Fig. 1c, d). Moreover, administration of IL-33 after metastatic engraftment, or intranasal sensitization with non-type-2-inducing
95 inflammatory agents (CpG or LPS) had no effect on metastatic seeding (Extended Data Fig. 1e, f). Next, we assessed the role of IL-33- or Asp-
96 sensitization in metastatic models of lung carcinoma (LL/2, C57BL/6J genetic background) and breast cancer (4T1, BALB/c genetic
97 background), which also showed increased tumor burden in mice exposed to innate type-2 inflammation (Fig. 1e, f). Similarly, both
98 orthotopically implanted 4T1 and highly metastatic 4T1-T breast cancer cells developed more lung metastases in mice exposed to intranasal
99 Asp or IL-33, without influencing primary tumor size (Fig. 1g, h, Extended Data Fig. 1g). In an autochthonous model of breast cancer
100 (B6.MMTV-PyMT) that metastasizes to the lung, IL-33 or Asp treatment similarly promoted lung metastases without affecting primary tumor
101 size (Fig. 1i, Extended Data Fig. 1h). Therefore, we conclude that IL-33- or allergen-driven type-2 airway inflammation significantly increases
102 lung metastatic burden in cancer.

103

104 Allergen exposure leads to IL-33 release, resulting in the rapid activation of ILC2 which subsequently contribute to innate and adaptive type-2
105 inflammation⁴. We confirm that intranasal IL-33 induces ILC2 expansion, and that Asp induces IL-33-dependent acute type-2 inflammation, as
106 measured by eosinophilia (Extended Data Fig. 1i, j, k). To investigate whether Asp-driven increases in lung metastases depend on IL-33, we
107 primed C57BL/6J wild type and *Il33*^{-/-} mice with Asp before adoptively transferring B16.F10 cells. While wild type mice treated with Asp had
108 significantly more lung metastases on day 21, we observed no effect of allergen treatment in *Il33*^{-/-} mice (Fig. 1j). As ILC2 are the primary lung
109 cells that respond to acute IL-33 release¹⁶, we hypothesized that ILC2 may promote metastatic seeding after IL-33 or allergen exposure. To test
110 this, we exposed *Il7ra*^{Cre/+}*Rora*^{fl/fl} ILC2-deficient⁵ or control mice to IL-33 or Asp allergen, followed by adoptive transfer of B16.F10 cells and
111 assessment of metastatic burden. Similar to *Il33*^{-/-} mice, ILC2-deficient mice produced significantly fewer lung metastases after exposure to
112 either IL-33 or Asp allergen compared to control mice (Fig. 1k, l). Hence, we propose that allergen-induced promotion of lung metastasis
113 formation is reliant on IL-33-driven activation of ILC2.

114

115 **IL-33 does not promote early seeding of the lung by CTC**

116

117 To determine whether IL-33-ILC2-dependent airway inflammation influences early arrest of CTC in the capillaries of inflamed lung, we
118 quantified either B16.F10-mCherry fluorescent, or B16.F10-Akaluc bioluminescent cells at early time-points in IL-33-primed or control mice. IL-
119 33-primed lungs were not seeded with more CTC (Fig. 2a, b), arguing that another mechanism may promote metastatic burden. NK cells are
120 essential for detecting and eliminating both CTC and early metastatic lesions². To investigate if IL-33 functions in a parallel pathway with NK
121 cells, we asked if IL-33 priming synergizes with NK cell depletion (Extended Data Fig. 2a). We first confirmed that NK cell depletion resulted in
122 a substantial increase in lung metastasis formation (Fig. 3a). Moreover, we observed no additive effect of IL-33 priming in NK cell depleted
123 mice; Thus, while IL-33 does not promote early arrest of CTC in the lung, we hypothesised that IL-33 influences NK cell-driven anti-tumor
124 function.

125

126 **IL-33 suppresses lung NK cell function**

127

128 NK cells are the major ILC population, and the predominant source of IFN γ in the lungs of naive mice, which is involved in the anti-metastatic
129 function of lung NK cells (Extended Data Fig. 2b)¹⁷. IL-33 administration moderately increased total lung NK cell numbers (Extended Data Fig.
130 2c). We confirmed that IL-33 administration induced expansion of ST2⁺ ILC2, while ST2⁻ lung NK cells did not increase Ki67 expression (Fig.
131 3b, Extended Data Fig. 2d), suggesting a potential indirect effect of IL-33 on NK cells. We next assessed the functional capacity of lung NK
132 cells in PBS or IL-33-treated mice by detection of intracellular IFN γ , Granzyme B (GzmB) and tumor necrosis factor (TNF). In IL-33-treated
133 mice, we observed a significant reduction in IFN γ production after *ex vivo* stimulation with either phorbol-12-myristate-13-acetate (PMA) plus
134 ionomycin (PI), or anti-NK1.1 antibody (Fig. 3c, Extended Data Fig 2e, f), and substantial reductions in total lung IFN γ -positive NK cell numbers
135 (Extended Data Fig. 2g). Additionally, we observed a significant reduction in GzmB and TNF production (Fig. 3d). Similar results were obtained
136 after *ex vivo* stimulation with a combination of IL-12 and IL-18 (Extended Data Fig. 2h). Intranasal IL-33-administration had no or minimal effect
137 on circulating or splenic NK cell function (Fig. 3e), although peri-cardiac adipose NK cells were suppressed (Extended Data Fig. 2i).

138

139 We investigated the kinetics of lung NK cell suppression in timecourse experiments, and found that IFN γ production was suppressed for about
140 2 weeks after intranasal IL-33 administration (blue), while intranasal LPS treated mice (grey) did not differ from baseline (black, d0) (Fig. 3f).
141 Suppression appeared inversely correlated with type-2 inflammation (Extended Data Fig. 1c). Notably, the capacity of lung CD4⁺ and CD8⁺ T
142 cells to produce IFN γ was unaffected by IL-33 treatment (Extended Data Fig. 2j). Moreover, IFN γ and GzmB production by purified NK cells
143 from naive mouse lungs was effectively suppressed upon co-culture with IL-33-treated lung cells, indicating that the lung inflammatory milieu
144 has potent immunosuppressive properties (Fig. 3g, Extended Data Fig. 2k). Conversely, purified NK cells from IL-33-treated lungs regained
145 IFN γ and GzmB expression upon co-culture with PBS-treated lung cells, indicating that suppression is reversible. Next, by *in vitro* cytotoxicity
146 assay, we found that lung NK cells from IL-33 mice were impaired in their ability to eliminate tumor cells (Fig. 3h).

147

148 To assess if allergen-induced IL-33 release could affect lung NK cells, we treated both wild type and *Il33*^{-/-} mice with PBS or Asp. Intranasal
149 Asp administration led to reduced lung NK cell function in wild type but not *Il33*^{-/-} mice on day 3 (Fig. 3i). Administration of ragweed pollen
150 similarly impaired lung NK cell function (Fig. 3j). We also observed suppression of CD49b⁺ NK cell function in BALB/c mice treated with IL-33
151 (Fig. 3k). Moreover, parallel experiments conducted on C57BL/6 mice in a different animal facility produced comparable results in terms of NK

152 cell suppression and increased metastatic seeding upon IL-33 treatment (Extended Data Fig. 2l, m). In all, these data suggest that allergen-
153 induced IL-33 release suppresses lung NK cell function.

154

155 **ILC2 mediate an innate-immune checkpoint on lung NK cell function**

156

157 As the main IL-33-responsive cell in naive lungs, ILC2 may orchestrate suppression of NK cells. Indeed, IL-33- or Asp-treated ILC2-deficient
158 mice failed to suppress production of IFN γ and GzmB by lung NK cells, or induce type-2 inflammation (Fig. 4a, Extended Data Fig. 3a). ILC2-
159 deficient mice that were also depleted of NK cells were now susceptible to increased metastatic seeding (Fig. 4b), supporting the hypothesis
160 that ILC2-mediated suppression of NK cells is important in promoting lung metastasis formation. Relatedly, IL-33-sensitization did not influence
161 metastatic seeding in NK cell depleted ILC2-deficient mice (Fig. 4b). While these data suggest that ILC2 can influence lung NK cell function,
162 possibly via a direct AMP-mediated pathway¹⁸, we found that both *in vitro* lung ILC2 and NK cell co-culture, as well as small molecule inhibition
163 of A2AR *in vivo* failed to suppress or rescue NK cell function respectively, indicating that another indirect mechanism may elaborate the NK
164 cell-suppressing function of ILC2 (Extended Data Fig. 3b, c, d).

165

166 ILC2 can promote both conventional and regulatory CD4⁺ T cell expansion in the lungs^{5, 6, 19, 20}. To ascertain if ILC2-mediated suppression of
167 NK cells relies on concomitant CD4⁺ T cell function, we used CD4-depleting antibody together with IL-33 treatment. However, neither lack of
168 CD4⁺ T cells nor neutralization of IL-10 or TGF- β could rescue IL-33-induced suppression of NK cells (Fig. 4c, Extended Data Fig. 3e).
169 Similarly, depletion of CD4⁺ T_{reg} cells (B6.*Foxp3^{DTR}*) did not impair the effect of IL-33 on lung NK cell suppression (Extended Data Fig. 3f). To
170 ask if other adaptive immune cells contribute to this phenotype, we administered IL-33 to both wild type, μ MT and *Rag2*^{-/-} mice, followed by
171 measurement of IFN γ production by lung NK cells. We found that lung NK cells in both wild type, μ MT and *Rag2*^{-/-} mice are similarly impaired
172 upon IL-33 treatment (Fig. 4d, e, left panels), suggesting that ILC2 collaborate with non-adaptive-immune cells to suppress NK cell function.
173 Moreover, IL-33 priming of *Rag2*^{-/-} mice followed by B16.F10 or LL/2 adoptive transfer resulted in a similar increase in metastatic burden
174 compared to IL-33-treated wild type mice (Fig. 4f, left panel, and Extended Data Fig. 3g). B16.F10 adoptive transfer into mice lacking both
175 adaptive and innate lymphocytes confirmed the important role of NK cells in preventing metastatic seeding of the lung, and also demonstrated

176 no additive effect of IL-33 sensitization in the absence of ILC (Fig. 4f, right panel). Lastly, we created ILC2-deficient mice on the *Rag2*^{-/-}
177 background (*Rag2*^{-/-}*Il7ra*^{Cre}*Rora*^{fl/fl}), which also failed to suppress NK cells in response to IL-33 (Fig. 4g, Extended Data Fig. 3h). Thus,
178 activated ILC2 can suppress NK cells via an innate-immune regulatory mechanism.

179

180 **ILC2-derived IL-5 promotes eosinophil-mediated suppression of lung NK cells**

181

182 Myeloid cells are implicated in promoting lung metastasis formation²¹, can suppress NK cells², and are induced or stimulated by ILC2,
183 advancing the hypothesis that a myeloid-ILC2 interaction elaborates IL-33-driven suppression of NK cells. We first characterized the myeloid
184 compartment in the lungs of PBS and IL-33 treated mice on day 3, which revealed an expected influx of eosinophils, inflammatory monocyte-
185 derived macrophages (IM) and dendritic cells, as well as neutrophils and monocytes (Extended Data Fig. 4a, b). Given the known immune-
186 suppressive functions of Gr-1⁺ (Ly-6G⁺ or Ly-6C⁺) myeloid cells^{22, 23}, we used antibody-mediated depletion to assess their role in IL-33-driven
187 suppression of NK cells. Anti-Gr-1 treatment reversed the effect of IL-33 on suppression of IFN γ and GzmB production by NK cells (Fig. 5a,
188 Extended Data Fig. 5a). However, parallel assessment of the myeloid compartment revealed that multiple immune cells were affected by anti-
189 Gr-1 treatment in IL-33-sensitized mice, including eosinophils, highlighting broad direct or indirect effects of this reagent (Fig 5a, Extended Data
190 Fig. 5a). Targeted depletion of Ly-6G⁺ neutrophils, or impairment of CCR2-CCL2-mediated influx of monocytes was largely unsuccessful in
191 reverting IL-33-driven suppression of NK cells (Extended Data Fig. 5b, c, d). Similarly, clodronate-liposome-mediated depletion of alveolar
192 macrophages (AM) failed to rescue NK cell suppression (Extended Data Fig. 5e). This suggested that neutrophils, despite their pro-metastatic
193 function in other models^{22, 24, 25} are not involved in IL-33-mediated suppression of lung NK cells.

194

195 We found lung eosinophilia to be most strongly correlated with suppression of IFN γ production by NK cells (Fig. 5b, Extended Data Fig. 4d).
196 Although surface Ly-6G-negative, eosinophils express Ly-6C (Extended Data Fig. 4c), and numbers were reduced in IL-33-sensitized lungs
197 upon anti-Gr-1 treatment (Fig. 5a). To specifically assess the role of eosinophils on NK cell suppression we neutralized IL-5, a cytokine
198 essential for eosinophilic inflammation²⁶, which is primarily secreted by ILC2 during innate type-2 lung inflammation (Extended Data Fig. 6a).
199 Lung eosinophil numbers were significantly reduced by anti-IL-5 treatment in IL-33-sensitized mice, while neutrophil numbers were unaffected

200 (Fig. 5c, Extended Data Fig. 6b, c). Moreover, anti-IL-5 treatment also did not impair other inflammatory effects of IL-33, such as alternative
201 activation of AM and (IM) as assessed by RELM α expression (Fig. 5d, e). Anti-IL-5 treatment protected against the suppressive effect of IL-33
202 on lung NK cell production of IFN γ and GzmB, after re-stimulation with both PI and anti-NK1.1 (Fig. 5c, Extended Data Fig. 6d).

203

204 Intranasal administration of recombinant IL-4, IL-13, IL-5, or GM-CSF did not induce lung eosinophilia or NK cell suppression, suggesting that
205 IL-5 is essential but not sufficient for NK cell suppression (Extended Data Fig. 6e). Indeed, it is known that IL-5 operates in concert with other
206 inflammatory mediators to promote lung eosinophilia²⁶. Relatedly, *IL5*^{-/-} mice develop fewer lung metastases²⁷, and we found prolonged survival
207 in PBS- or Asp-treated *IL33*^{-/-} mice after B16.F10 transfer (Extended Data Fig. 6f). Moreover, adoptive transfer of eosinophils to naive mice, or
208 co-culture of NK cells with *ex vivo* derived or purified lung eosinophils from IL-33 treated mice effectively suppressed lung NK cell function,
209 whereas cDC2, IM and AM did not (Fig. 5f, g, Extended Data Fig. 6g). Notably, both naive and inflamed lung eosinophils do not express ST2,
210 and no additive effect of IL-33 on NK cell–eosinophil co-cultures was observed (Fig. 5h, i). These data indicate that ILC2-derived IL-5 is
211 important for eosinophil-mediated suppression of NK cell function.

212

213 **IL-33-induced suppression of lung NK cell effector molecules is not transcriptionally regulated**

214

215 To investigate how lung NK cells were affected in terms of gene regulation, we performed single-cell-RNA-seq analysis on flow cytometry
216 purified lung NK cells from PBS or IL-33 treated wild type mice at different time-points (Extended Data Fig. 7a, b). At day 3, we identified 7
217 clusters (*see Methods*) of NK cells in PBS and IL-33-treated lungs in single-cell RNA-seq data (Fig. 6a), which were annotated by their gene
218 expression patterns and assessed for maturation and proliferation markers. Cluster 7 exhibits signatures indicative of CD27^{hi}CD11b^{low}
219 immature NK cells, whose relative abundance corresponds with our flow cytometry observations (Extended Data Fig. 7c, d). Comparison of
220 treatment arms did not reveal the emergence of novel clusters, but suggested shifts in relative proportions of clusters and subtle global
221 changes in gene expression across clusters upon IL-33 treatment (Fig. 6b, c, Extended Data Fig. 7e). In contrast to protein expression
222 measurements, effector molecule genes such as *Irfng* and *Gzmb* were either unaffected or upregulated by IL-33 treatment, respectively.

223

224 We also performed a bulk-RNA-seq time-course on lung NK cells after IL-33 administration to capture changes in gene transcription over time
225 (Extended Data Fig. 7a). We tested if IL-33-treatment led to changes in expression of NK cell consensus, effector molecule, or activating and
226 inhibitory receptor gene-sets. We did not observe substantial modulation in expression at 2, 7 or 14 days after intranasal IL-33 administration
227 (n=3), or on day 3 in a higher-powered (n=6, 7) bulk-RNA-seq experiment (Fig. 6d, e, Extended Data Fig. 7f, g). Altogether, these
228 transcriptomic studies suggest that post-transcriptional regulation may influence the functional impairment of lung NK cells after IL-33
229 administration.

230

231 **Activated ILC2 suppress NK cells via an eosinophil-mediated metabolic mechanism**

232

233 As post-transcriptional regulation of NK cell function can be controlled by their metabolic state²⁸, we hypothesized that global suppression of lung
234 NK cell function is influenced by eosinophil-induced changes in NK cell metabolism. Metabolic stress is sensed by NK cells, resulting in
235 suppressed mTORC1-activity, and reduced phosphorylation of ribosomal subunit S6²⁹. We observed reduced phospho-S6 levels in IL-33- or
236 Asp-treated lung NK cells upon stimulation (Fig. 7a, b). Phospho-S6 levels were unchanged in Asp-treated ILC2-deficient mice, and restored
237 upon IL-5-neutralisation in IL-33-treated wild type mice (Fig. 7c, d). Moreover, metabolic profiling of lung cultures by nuclear magnetic
238 resonance (NMR) revealed an increase in glucose utilization upon IL-33 treatment (Fig. 7e). Activated eosinophils primarily utilize glycolysis³⁰,
239 and express associated metabolic pathway genes, including glucose transporters Glut1 and Glut3 (encoded by genes *Slc2a1*, *Slc2a3*)³¹.
240 Correspondingly, we observed uptake of the 2-NBDG glucose analog by lung eosinophils, which increased in IL-33-treated mice (Fig. 7f).
241 Importantly, IL-5-neutralisation reversed IL-33 mediated changes in glucose utilization and lactate production in both C57BL/6J and BALB/c
242 mice (Fig. 7g, Extended Data Fig. 8a). Additionally, mass spectrometry imaging (MSI) of mice infused with [U-¹³C] glucose was performed to
243 assess *in vivo* glycolysis in inflamed lungs (Fig. 7h, Extended Data Fig. 8b, c, d). We observed increased [U-¹³C] and [U-¹²C] lactate/glucose
244 ratios upon IL-33 treatment in wild type but not ILC2-deficient mice (Fig. 7i, Extended Data Fig. 8b, c, d). These data support the hypothesis
245 that ILC2-induced eosinophilia modulates glucose utilization in the lung environment.

246

247 We further tested if depletion of glucose or increased concentrations of lactate were responsible for impaired NK cell function. We found that
248 glucose restriction impaired naive lung NK cell function, while high glucose media rescued IFN γ and GzmB production, as well as phospho-S6
249 expression, by IL-33-treated lung NK cells upon activation (Fig. 7j, k). Moreover, *ex vivo* activated NK cells from IL-33-treated mouse lungs
250 exhibit an increased extracellular acidification rate (ECAR) after glucose administration (Fig. 7l). Gene set enrichment analysis (GSEA)
251 identified enrichment of genes associated with glycolysis in the IL-33-treated lung NK cells compared to PBS control (Fig. 7m). Interestingly,
252 culture of naive lung NK cells in lactic acid suppressed IFN γ but not GzmB production (Fig. 7n). These data suggest that ILC2-induced
253 eosinophilia orchestrates suppression of NK cell function by restraining NK cell glucose metabolism.

254

255 **Therapeutic targeting of the ILC2-eosinophil axis restores NK cell-mediated tumor control**

256

257 As we have observed that IL-33-driven activation of ILC2 represents a central node in a mechanism of type-1 immunity regulation, we
258 postulated that this axis may present a potential therapeutic target. Given that IL-5- and IL-33-targeted therapeutics are already in the clinic or
259 undergoing phase-2 clinical trials, respectively³², we first utilized an IL-33 trap (IL-33R-Fc) to block Asp allergen-induced airway inflammation.
260 Prophylactic dosing prevented NK cell suppression in wild type mice upon Asp administration, while also reducing markers of type-2
261 inflammation, including eosinophilic inflammation (Fig. 8a). Similarly, Asp-induced metastatic burden of B16.F10 melanoma was alleviated
262 upon IL-33 neutralization (Fig. 8b, c). In addition to anti-IL-5 restoring NK cell function (Fig. 5c), we find that prophylactic administration
263 significantly reduced the metastatic burden in both Asp- and IL-33-sensitized mice, upon transfer B16.F10 cells (Fig. 8b, c, d). We further
264 administered anti-IL-5 to BALB/c mice bearing 4T1 or 4T1-T orthotopically implanted breast cancer cells, and found a reduction in lung
265 metastases formation in Asp-treated groups, but no effect on primary tumor burden (Fig. 8e, Extended Data Fig. 8e, f). Moreover, given that
266 BALB/c mice are predisposed towards both innate and adaptive type-2 inflammation³³, we investigated if prophylactic dosing may reduce
267 metastasis formation in naive mice; We observe that both IL-5- or IL-33-neutralization reduced lung metastases in a model of metastasis from
268 primary breast cancer (Fig 8f). Thus, targeting of the ILC2-eosinophil axis can restore anti-mestastic function of lung NK cells (Extended Data
269 Fig. 8g).

270

271 **Discussion**

272

273 In summary, our data implicates ILC2-driven innate type-2 inflammation in promoting metastatic seeding of the airways. We find that ILC2 can
274 locally antagonize lung NK cell function via an eosinophil-mediated metabolic checkpoint. Therapeutic or genetic interference in this pathway
275 restores NK cell functionality, with benefit on tumor burden.

276

277 Both primary tumor-derived and exogenous factors that promote inflammation can influence CTC arrest in the pre-metastatic niche^{1, 21}. We
278 found that ILC2-driven inflammation had no effect on mechanical trapping of CTC, but did acutely suppress lung NK cell function. Against our
279 expectations, adaptive immune cells did not play a major role, while targeting of eosinophils was effective in reversing the effect of IL-33 on NK
280 cells. Although neutrophils are also known to enhance CTC extravasation and lung metastasis formation^{22, 34}, we found that specific ablation
281 was ineffective at blocking IL-33-mediated NK cell suppression. Conversely, anti-IL-5 mAb treatment targeted eosinophils specifically, and
282 reduced both NK cell suppression and metastatic seeding of the lung. Nevertheless, eosinophils are also reported to have anti-metastatic
283 function in the lung³⁵. However, our studies use 10-to-20 fold less IL-33, or use physiological stimuli in conjunction with *Il33*^{-/-} mice to reveal a
284 pro-metastatic role in six different tumor models on different genetic backgrounds, and in different animal facilities. While eosinophils are
285 primarily associated with type-2 inflammatory diseases, little is known about their ability to suppress type-1 immunity²⁶.

286

287 Type-1 cytokines can directly antagonize effector functions of adaptive and innate type-2 lymphocytes^{6, 36}. Reciprocal type-2 cytokine-driven
288 regulatory mechanisms are less well defined, although IL-4 can suppress IFN γ production at very early stages of T cell activation³⁷. Moreover,
289 T_{reg} cells and recently identified ILC_{reg} are known to restrain type-1 immune cells via production of IL-10 or TGF- β ^{8, 38, 39}, however we found that
290 these cytokines, or adaptive immunity, did not play a significant role in ILC2-mediated suppression of NK cells. While the ILC2-eosinophil-
291 driven innate immune checkpoint suppresses anti-metastatic function of NK cells, its effect on adaptive anti-tumor immunity remains unknown.
292 B16.F10 and other cancer cell-lines are susceptible to mono- and combination-immunotherapy⁴⁰, prompting future studies to assess the role of
293 ILC2-driven suppression on adaptive anti-tumor immunity.

294

295 IL-33 primarily promotes both innate and adaptive type-2 immunity, although there are reports of IL-33 directly stimulating NK and CD8⁺ T
296 cells^{41, 42, 43}. However, our results in ILC2-deficient or anti-IL-5 treated mice reveal indirect suppression by IL-33 on innate type-1 immunity.
297 Nevertheless, forced overexpression of *Il33* by tumors, or prolonged administration of high-dose IL-33 can promote anti-tumor immunity via
298 indirect mechanisms that involve ILC2 in the primary tumor environment^{13, 44}. Our data reveal a critical role of ILC2 and IL-33 in the pre-
299 metastatic niche, which may stimulate further studies that disentangle physiological and therapy-induced effects of IL-33 at both the primary
300 tumor and peripheral sites. Moreover, as our IL-33 neutralization and *Il33*^{-/-} mouse experiments target the endogenous release of IL-33, we
301 speculate that ILC2-mediated innate type-1 immune suppression may influence other physiological roles such as lipid metabolism and wound
302 healing; Indeed, IL-33 can also suppress adipose tissue NK cells.

303

304 IL-5 is primarily known for its importance in eosinophil development and function⁴⁵. Our neutralization experiments reveal an essential role for
305 IL-5 in mediating ILC2-dependent NK cell suppression. Importantly, IL-5 alone is not sufficient for exerting this function, and likely works in
306 concert with other IL-33-induced factors that promote eosinophilic inflammation such as IL-13 and eotaxins^{26, 46}. By neutralizing endogenously
307 produced IL-5 (and IL-33), we target a physiological pathway that complements experiments using ILC2-deficient mice, which lack the primary
308 innate source of IL-5 in the airways. Similarly, these approaches identify eosinophils as the critical myeloid cell-type that collaborates with ILC2
309 to suppress NK cell function. It remains to be determined whether ILC2, or other sources of IL-5 such as T_H2 or mast cells exert similar control
310 over NK cells in other organs.

311

312 Unexpectedly, we found that suppression of lung NK cell effector function did not coincide with major changes in transcription of core NK cell
313 genes, or shifts in lung NK cell clusters, after IL-33 administration. However, post-transcriptional regulation of NK cell function can be governed
314 by the activation-induced metabolic demand, and extracellular metabolite concentrations²⁸. Although functionally and metabolically quiescent at
315 rest, *ex vivo* activation resulted in increased glycolysis of NK cells from IL-33-treated lungs. Consistent with this, naive NK cells are initially
316 more reliant on OXPHOS for effector function⁴⁷, raising the possibility that the inflammatory environment provides signals that increase their
317 reliance on glycolysis²⁹. Increased reliance on glycolysis of lung NK cells coincides with altered metabolite bioavailability in the IL-33-treated

318 lung milieu. Low concentrations of glucose, or lactate acidosis, impairs effector functions of NK and other lymphoid cells^{28, 48}. Lung eosinophils
319 are likely responsible for local glucose depletion and production of lactic acid in the IL-33-inflamed setting; Eosinophils are the most prevalent
320 myeloid population in the inflamed lungs and readily take up 2-NBDG, while *ex vivo* cultures of inflamed lung utilise glucose and secrete lactate
321 more than uninflamed lungs, which is reversed by anti-IL-5-mediated prevention of eosinophilia. The implications of glucose depletion or lactic
322 acidosis on naive lung NK cell function is confirmed by our observed reductions in phospho-S6, and downstream translation of effector
323 molecules. This mirrors the phenotype of NK cells from inflamed lungs, while reduced phospho-S6 and effector molecule production can be
324 rescued by the genetic or therapeutic blockade of eosinophilia. Similarly, suppressed lung NK cells can be partially rescued by culture in high-
325 glucose conditions. Lastly, using MSI of [U-¹³C]glucose infused mice we demonstrate that IL-33 increases glucose flux in the inflamed lung
326 environment. These findings support the concept of nutrient competition in the immune-microenvironment⁴⁹. It remains unknown what NK cell-
327 intrinsic mechanisms are responsible for sensing metabolite availability, although in CD8⁺ T cells AMPK α 1 can sense glucose availability to
328 modulate mTORC1 and S6k⁵⁰. Thus, we provide compelling evidence that ILC2-driven lung eosinophilia modulates the extracellular availability
329 of metabolites, which impairs efficient glycolysis-dependent effector functions of lung NK cells.

330

331 **Accession codes**

332 Transcriptomic data is available at the Sequence Read Archive (SRA) under the Bioproject PRJNA637311.

333

334 **Acknowledgements**

335

336 We acknowledge the following funding sources: EMBO long-term post-doctoral fellowship (ALTF 423-2017, MJS), MRC Skills Development
337 Fellowship (MR/P014178/1, ACR), European Union's Horizon 2020 research and innovation programme under the Marie Skłodowska-Curie
338 grant agreement (PanILC No 840501, JS), The Royal Society and Wellcome Trust (204622/Z/16/Z, TYH), Cancer Research UK (CRUK) core
339 award (A24995, TYH), and the CRUK Grand Challenge Rosetta Consortium (C197/A25040, KMB, RJAG, AT and GH). DESI-MSI optimization

340 was supported by N Strittmatter. We thank the CRUK-CI research instrumentation, flow cytometry, genomics, bioinformatics, histopathology,
341 imaging and BRU cores for their expertise and help.

342

343 **Author Contributions**

344

345 MJS designed and conducted experiments, and wrote the manuscript. SP, ACR, AT, GH, SiP, CG, AN, JuS, JiS, AR and EMS assisted with
346 experiments or analysis. JDS, MDE, ANJM, HR, MM, GJH, XRR, SC, RJAG, KMB and JM provided reagents and/or advice. TYH supervised
347 the study, designed and conducted experiments, and wrote the manuscript.

348

349 **Competing Interests Statement**

350

351 GH, XRR, RJAG and ESC are employees of AstraZeneca and have stock/stock options in AstraZeneca.

352

353 **References**

- 354 1. Steeg, P.S. Targeting metastasis. *Nat Rev Cancer* **16**, 201-218 (2016).
355
- 356 2. Lopez-Soto, A., Gonzalez, S., Smyth, M.J. & Galluzzi, L. Control of Metastasis by NK Cells. *Cancer Cell* **32**, 135-154 (2017).
357
- 358 3. Monticelli, L.A. *et al.* Innate lymphoid cells promote lung-tissue homeostasis after infection with influenza virus. *Nat Immunol* **12**,
359 1045-1054 (2011).
360
- 361 4. Schuijs, M.J. & Halim, T.Y.F. Group 2 innate lymphocytes at the interface between innate and adaptive immunity. *Ann N Y Acad Sci*
362 **1417**, 87-103 (2018).
363
- 364 5. Halim, T.Y.F. *et al.* Tissue-Restricted Adaptive Type 2 Immunity Is Orchestrated by Expression of the Costimulatory Molecule
365 OX40L on Group 2 Innate Lymphoid Cells. *Immunity* **48**, 1195-1207 e1196 (2018).
366
- 367 6. Molofsky, A.B. *et al.* Interleukin-33 and Interferon-gamma Counter-Regulate Group 2 Innate Lymphoid Cell Activation during
368 Immune Perturbation. *Immunity* **43**, 161-174 (2015).
369
- 370 7. Crome, S.Q. *et al.* A distinct innate lymphoid cell population regulates tumor-associated T cells. *Nat Med* **23**, 368-375 (2017).
371
- 372 8. Wang, S. *et al.* Regulatory Innate Lymphoid Cells Control Innate Intestinal Inflammation. *Cell* **171**, 201-216 e218 (2017).
373
- 374 9. Seehus, C.R. *et al.* Alternative activation generates IL-10 producing type 2 innate lymphoid cells. *Nat Commun* **8**, 1900 (2017).
375
- 376 10. Fournie, J.J. & Poupot, M. The Pro-tumorigenic IL-33 Involved in Antitumor Immunity: A Yin and Yang Cytokine. *Front Immunol* **9**,
377 2506 (2018).
378
- 379 11. Chevalier, M.F. *et al.* ILC2-modulated T cell-to-MDSC balance is associated with bladder cancer recurrence. *J Clin Invest* **127**,
380 2916-2929 (2017).
381
- 382 12. Jovanovic, I.P. *et al.* Interleukin-33/ST2 axis promotes breast cancer growth and metastases by facilitating intratumoral
383 accumulation of immunosuppressive and innate lymphoid cells. *Int J Cancer* **134**, 1669-1682 (2014).

- 384
385 13. Saranchova, I. *et al.* Type 2 Innate Lymphocytes Actuate Immunity Against Tumours and Limit Cancer Metastasis. *Sci Rep* **8**, 2924
386 (2018).
387
- 388 14. DeNardo, D.G. *et al.* CD4(+) T cells regulate pulmonary metastasis of mammary carcinomas by enhancing protumor properties of
389 macrophages. *Cancer Cell* **16**, 91-102 (2009).
390
- 391 15. Taranova, A.G. *et al.* Allergic pulmonary inflammation promotes the recruitment of circulating tumor cells to the lung. *Cancer Res*
392 **68**, 8582-8589 (2008).
393
- 394 16. Halim, T.Y., Krauss, R.H., Sun, A.C. & Takei, F. Lung natural helper cells are a critical source of Th2 cell-type cytokines in protease
395 allergen-induced airway inflammation. *Immunity* **36**, 451-463 (2012).
396
- 397 17. Street, S.E., Cretney, E. & Smyth, M.J. Perforin and interferon-gamma activities independently control tumor initiation, growth,
398 and metastasis. *Blood* **97**, 192-197 (2001).
399
- 400 18. Long, A. *et al.* Type 2 Innate Lymphoid Cells Impede IL-33-Mediated Tumor Suppression. *J Immunol* **201**, 3456-3464 (2018).
401
- 402 19. Halim, T.Y. *et al.* Group 2 innate lymphoid cells license dendritic cells to potentiate memory TH2 cell responses. *Nat Immunol* **17**,
403 57-64 (2016).
404
- 405 20. Halim, T.Y. *et al.* Group 2 innate lymphoid cells are critical for the initiation of adaptive T helper 2 cell-mediated allergic lung
406 inflammation. *Immunity* **40**, 425-435 (2014).
407
- 408 21. Altorki, N.K. *et al.* The lung microenvironment: an important regulator of tumour growth and metastasis. *Nat Rev Cancer* **19**, 9-31
409 (2019).
410
- 411 22. Coffelt, S.B. *et al.* IL-17-producing gammadelta T cells and neutrophils conspire to promote breast cancer metastasis. *Nature* **522**,
412 345-348 (2015).
413
- 414 23. Gabrilovich, D.I. Myeloid-Derived Suppressor Cells. *Cancer Immunol Res* **5**, 3-8 (2017).
415

- 416 24. Albregues, J. *et al.* Neutrophil extracellular traps produced during inflammation awaken dormant cancer cells in mice. *Science*
417 **361** (2018).
418
- 419 25. Quail, D.F. *et al.* Obesity alters the lung myeloid cell landscape to enhance breast cancer metastasis through IL5 and GM-CSF. *Nat*
420 *Cell Biol* **19**, 974-987 (2017).
421
- 422 26. Weller, P.F. & Spencer, L.A. Functions of tissue-resident eosinophils. *Nat Rev Immunol* **17**, 746-760 (2017).
423
- 424 27. Zaynagetdinov, R. *et al.* Interleukin-5 facilitates lung metastasis by modulating the immune microenvironment. *Cancer Res* **75**,
425 1624-1634 (2015).
426
- 427 28. O'Brien, K.L. & Finlay, D.K. Immunometabolism and natural killer cell responses. *Nat Rev Immunol* **19**, 282-290 (2019).
428
- 429 29. Donnelly, R.P. *et al.* mTORC1-dependent metabolic reprogramming is a prerequisite for NK cell effector function. *J Immunol* **193**,
430 4477-4484 (2014).
431
- 432 30. Porter, L. *et al.* Metabolic Profiling of Human Eosinophils. *Front Immunol* **9**, 1404 (2018).
433
- 434 31. Fairfax, K.A. *et al.* Transcriptional profiling of eosinophil subsets in interleukin-5 transgenic mice. *J Leukoc Biol* **104**, 195-204
435 (2018).
436
- 437 32. Lawrence, M.G., Steinke, J.W. & Borish, L. Cytokine-targeting biologics for allergic diseases. *Ann Allergy Asthma Immunol* **120**,
438 376-381 (2018).
439
- 440 33. Hsieh, C.S., Macatonia, S.E., O'Garra, A. & Murphy, K.M. T cell genetic background determines default T helper phenotype
441 development in vitro. *Journal of Experimental Medicine* **181**, 713-721 (1995).
442
- 443 34. Wculek, S.K. & Malanchi, I. Neutrophils support lung colonization of metastasis-initiating breast cancer cells. *Nature* **528**, 413-
444 417 (2015).
445
- 446 35. Lucarini, V. *et al.* IL-33 restricts tumor growth and inhibits pulmonary metastasis in melanoma-bearing mice through eosinophils.
447 *Oncoimmunology* **6**, e1317420 (2017).

- 448
449 36. Iwamoto, I., Nakajima, H., Endo, H. & Yoshida, S. Interferon gamma regulates antigen-induced eosinophil recruitment into the
450 mouse airways by inhibiting the infiltration of CD4+ T cells. *J Exp Med* **177**, 573-576 (1993).
451
- 452 37. Tanaka, T., Hu-Li, J., Seder, R.A., Fazekas de St Groth, B. & Paul, W.E. Interleukin 4 suppresses interleukin 2 and interferon gamma
453 production by naive T cells stimulated by accessory cell-dependent receptor engagement. *Proc Natl Acad Sci U S A* **90**, 5914-5918
454 (1993).
455
- 456 38. Li, M.O., Wan, Y.Y. & Flavell, R.A. T cell-produced transforming growth factor-beta1 controls T cell tolerance and regulates Th1-
457 and Th17-cell differentiation. *Immunity* **26**, 579-591 (2007).
458
- 459 39. Asseman, C., Mauze, S., Leach, M.W., Coffman, R.L. & Powrie, F. An essential role for interleukin 10 in the function of regulatory T
460 cells that inhibit intestinal inflammation. *J Exp Med* **190**, 995-1004 (1999).
461
- 462 40. Korman, A.J., Peggs, K.S. & Allison, J.P. Checkpoint blockade in cancer immunotherapy. *Adv Immunol* **90**, 297-339 (2006).
463
- 464 41. Bonilla, W.V. *et al.* The alarmin interleukin-33 drives protective antiviral CD8(+) T cell responses. *Science* **335**, 984-989 (2012).
465
- 466 42. Bourgeois, E. *et al.* The pro-Th2 cytokine IL-33 directly interacts with invariant NKT and NK cells to induce IFN-gamma
467 production. *Eur J Immunol* **39**, 1046-1055 (2009).
468
- 469 43. Qi, L. *et al.* Interleukin-33 activates and recruits natural killer cells to inhibit pulmonary metastatic cancer development. *Int J*
470 *Cancer* **146**, 1421-1434 (2020).
471
- 472 44. Moral, J.A. *et al.* ILC2s amplify PD-1 blockade by activating tissue-specific cancer immunity. *Nature* **579**, 130-135 (2020).
473
- 474 45. Dougan, M., Dranoff, G. & Dougan, S.K. GM-CSF, IL-3, and IL-5 Family of Cytokines: Regulators of Inflammation. *Immunity* **50**, 796-
475 811 (2019).
476
- 477 46. Mishra, A. & Rothenberg, M.E. Intratracheal IL-13 induces eosinophilic esophagitis by an IL-5, eotaxin-1, and STAT6-dependent
478 mechanism. *Gastroenterology* **125**, 1419-1427 (2003).
479

- 480 47. Keppel, M.P., Saucier, N., Mah, A.Y., Vogel, T.P. & Cooper, M.A. Activation-specific metabolic requirements for NK Cell IFN-gamma
481 production. *J Immunol* **194**, 1954-1962 (2015).
482
- 483 48. Brand, A. *et al.* LDHA-Associated Lactic Acid Production Blunts Tumor Immunosurveillance by T and NK Cells. *Cell Metab* **24**, 657-
484 671 (2016).
485
- 486 49. Kedia-Mehta, N. & Finlay, D.K. Competition for nutrients and its role in controlling immune responses. *Nat Commun* **10**, 2123
487 (2019).
488
- 489 50. Rolf, J. *et al.* AMPKalpha1: a glucose sensor that controls CD8 T-cell memory. *Eur J Immunol* **43**, 889-896 (2013).
490

491 **Figure Legends:**

492

493 **Figure 1 IL-33-driven activation of ILC2 is critical for promoting lung metastases**

494

495 **a-d**, Wild type (WT) mice were treated intranasally with IL-33, *Aspergillus* protease-allergen (Asp) or PBS, followed by intravenous transfer of
496 metastatic B16.F10 cells, and sacrifice on day 21 (**a**), and: visual quantification of lung metastases (**b**) (n = 11), histological staining for Ki67⁺
497 tumor cells (**c**), or kept alive to determine lung metastases-related mortality (**d**). **e, f** Lung metastases were visually quantified in mice treated as
498 in *Fig. 1a* with LL/2 (**e**) (n = 10,9,8), or 4T1 cells (**f**) (n = 10). **g,h**, 4T1 (**g**) (n = 10) or 4T1-T (**h**) (n = 13,14,10) breast cancer cells were
499 implanted in the mammary fat pad of BALB/c mice on day 0, followed by intranasal treatment with IL-33, Asp or PBS on days 7 and 14, and
500 visual quantification of lung metastases on day 21. **i**, Twelve-week-old female B6.MMTV-PyMT mice were randomized and treated intranasally
501 with IL-33, Asp or PBS once a week and sacrificed at 20 weeks of age, followed by visual quantification of lung metastases (n = 10,10,11). **j-l**,
502 WT and *Il33*^{-/-} mice (**j**; n = 10), or *Il7ra*^{Cre/+} and *Il7ra*^{Cre/+}*Rora*^{fl/fl} mice were treated as in *Fig. 1a* with IL-33 (**k**, n = 10,10,7,7) or Asp (**l**, n =
503 5,5,7,7) followed by visual quantification of lung metastases.

504

505 Bar graphs indicate mean (±SEM) and show combined data of two (d-h, and j-k) or three (b and i), or are representative of three independent
506 experiments (c and l). Statistical analyses were calculated using one-way ANOVA or Log-rank (Mantel-Cox) test (d) with **** = p ≤ 0.0001.

507

508

509 **Figure 2 IL-33 does not promote early seeding of the lung by CTC**

510

511 **a,b**, Albino C57BL/6 mice were treated intranasally with IL-33 or PBS on days 0 and 1, followed by intravenous transfer on day 7 of: (**a**)
512 substrate-conditioned B16.F10-AkaLuc cells, followed by IVIS imaging at the indicated times (representative image at 10 minutes), followed by
513 quantification of signal in the chest of mice (n = 8); (**b**) B16.F10-mCherry cells, followed by quantification of total B16.F10 tumor cells in the lung
514 24 hours after injection (n = 10). Representative gating shown for non-injected control (Ctrl) and B16.F10-mCherry cell injected (B16) mice.

515

516 Bar graphs indicate mean (±SEM) and show combined data of two independent experiments (a and b), IVIS and flow cytometry plots show
517 representative images of two independent experiment (a and b). Statistical analyses were calculated using unpaired two-tailed Student's t-test
518 (b) with ns = not significant.

519

520 **Figure 3 IL-33 suppresses lung NK cell function**

521

522 **a**, WT mice treated as in *Fig. 1a* were given anti-NK1.1 or control antibody, followed by visual quantification of lung metastases on day 21 (n =
523 10). **b-e**, WT mice were treated with IL-33 or PBS on day 0 and 1, followed by sacrifice on day 3 and: (**b**) ST2 expression by lung ILC2 and NK
524 cells was measured; (**c**) Identification (left) and quantification (right) of total IFN γ ⁺ lung NK cells after PI (top; n = 6,7) or anti-NK1.1(bottom; n =
525 3) stimulation; (**d**) Quantification of Gzmb⁺ and TNF⁺ lung NK cells (n = 10); (**e**) Quantification IFN γ ⁺ NK cells from listed anatomical sites (n =
526 5). **f**, Quantification of IFN γ ⁺ lung NK cells at the indicated time-points after intranasal treatment with IL-33 (blue) or LPS (grey) on day 0 and 1,
527 compared to PBS-treated WT animals (d0, black) (n = 6). **g**, Lung NK cells from PBS- or IL-33-treated WT mice were co-cultured for 12 hours
528 with CFSE labeled whole lung cell homogenates from PBS- or IL-33-treated WT mice. CFSE⁺ endogenous NK (grey) or purified NK (green,
529 blue) cells were subsequently assessed for IFN γ production (n = 6,11,10,10,2,5). **h**, Killing assay of YAC-1 target cells by lung NK cells from
530 PBS- or IL-33-treated WT mice (n = 3). **i**, WT and *Il33*^{-/-} mice were treated with Asp on day 0 and 1, followed by quantification of IFN γ ⁺ lung NK
531 cells on day 3 (n = 10,10,5,10). **j**, WT mice were treated with ragweed pollen (RWP), followed by quantification of IFN γ ⁺ and Gzmb⁺ lung NK
532 cells (n = 4,6). **k**, BALB/c mice were treated, as in *Fig. 3b*, followed by quantification of IFN γ ⁺ lung NK cells (n = 5).

533

534 Fluorescence-minus-one (FMO); Arbitrary unit (a.u.); Unless otherwise indicated PI re-stimulation was used to measure NK cell cytokine
535 production. Bar graphs indicate mean (\pm SEM) and show combined data of two (d,i) or three (a) independent experiments or a representative of
536 three independent experiments (b, c, e-h, j, k). Statistical analyses were calculated using one-way ANOVA, unpaired two-tailed Student's t-test
537 (c), or Wilcoxon matched-pairs signed rank (h) with **** = $p \leq 0.0001$.

538

539

540 **Figure 4 ILC2 mediate an innate-immune checkpoint on lung NK cell function**

541

542 **a,b**, *Il7ra*^{Cre/+} and *Il7ra*^{Cre/+}*Rora*^{fl/fl} mice were treated with PBS or IL-33 on day 0 and 1, followed by quantification of IFN γ ⁺ and Gzmb⁺ lung NK
543 cells, and lung eosinophilia on day 3 (**a**) (n = 6,6,6,7), or treated as in *Extended Data Fig. 2a*, followed by visual quantification of lung
544 metastases (**b**) (n = 10,10,7,8). **c**, WT mice were treated with PBS or IL-33 on day 0 and 1, and the indicated mAb on day -1 and 1 followed by
545 quantification of IFN γ ⁺ lung NK cells on day 3 (n = 6). **d**, WT and *Rag2*^{-/-} mice were treated with PBS or IL-33 on day 0 and 1, followed by
546 quantification of IFN γ ⁺ lung NK cells (left, n = 8,8,7,7) and lung eosinophilia (right, n = 3) on day 5. **e**, WT and μ MT mice were treated with PBS

547 or IL-33 on day 0 and 1, followed by quantification of IFN γ ⁺ lung NK cells (left, n = 10,10,10,11) and lung eosinophilia (right, n = 10,10,10,11) on
548 day 3. **f**, WT, *Rag2*^{-/-} (left, n = 5,5,5,6) and NOD/SCID.*Il2rg*^{-/-} (NSG) (right, n = 9) mice were treated as in *Fig. 1a*, followed by visual
549 quantification of lung metastases. **g**, Mice of indicated genotypes were treated with PBS or IL-33 on day 0 and 1, followed by quantification of
550 IFN γ ⁺ lung NK cells day 3 (n = 5,5,4,5,4,5).

551

552 PI re-stimulation was used to measure NK cell cytokine production. Bar graphs indicate mean (\pm SEM). Data shown are combined from two (c-
553 e) or three (b and f) independent experiments, or a representative of three independent experiments (a). Statistical analyses were calculated
554 using one-way ANOVA or unpaired two-tailed Student's t-test t (c) with ns = not significant, **** = p \leq 0.0001.

555

556 **Figure 5 ILC2-derived IL-5 promotes eosinophil-mediated suppression of lung NK cells**

557

558 **a**, WT mice were treated with PBS or IL-33 on day 0 and 1, and anti-Gr-1 or control antibody on day -1 and 1 followed by quantification of IFN γ ⁺
559 lung NK cells and eosinophil numbers (n = 15,14,14,15) on day 3. **b**, Correlation of lung eosinophil numbers and percent IFN γ ⁺ NK cells on day
560 3 from WT mice treated with PBS and IL-33- (days 0, 1) (n=125). **c-e**, WT mice were treated with PBS or IL-33 on day 0 and 1, and anti-IL-5 or
561 control antibody on day -6, -3 and -1 followed by quantification of IFN γ ⁺ and GzmB⁺ lung NK cells and eosinophilia (**c**) (n = 10), or flow
562 cytometric identification (**d**) and quantification of RELM α ⁺ AM and IM (**e**) (n = 5) on day 3. **f**, Eosinophils were adoptively transferred to WT mice
563 on day 0, followed by quantification of IFN γ ⁺ and GzmB⁺ lung NK cells and lung eosinophilia on day 1 (n = 10). **g**, Flow-cytometry sorted
564 immune cells from WT mice were co-cultured with purified lung NK cells for 12 hours followed by quantification of GzmB⁺ lung NK cells (n =
565 8,8,7,7,7). **h**, ST2 expression by WT mouse lung eosinophils on day 3 after treatment with PBS or IL-33 (day 0 and 1). **i**, WT mouse lung NK
566 cells were co-cultured for 12 hrs with eosinophils (1:10 ratio) with addition of IL-33 or control, followed by quantification of IFN γ ⁺ and GzmB⁺
567 lung NK cells (n = 6).

568

569 PI re-stimulation was used to measure NK cell cytokine production. Bar graphs indicate mean (\pm SEM). Data shown are combined from two (c-
570 e, and g- i) or three (a and f) independent experiments, with (gG) representing Pearson r (n=125). Statistical analyses were calculated using
571 one-way ANOVA or unpaired two-tailed Student's t-test (f) ns = not significant, **** = p \leq 0.0001.

572

573 **Figure 6 IL-33-induced suppression of lung NK cells is not transcriptionally regulated**

574

575 **a**, WT mice were treated with IL-33 or PBS on day 0 and 1, followed by isolation of lung NK cells on day 3 for scRNA-seq analysis. UMAP
576 projection of NK cell scRNA-seq data from 2 mice from each treatment coloured by treatment (left) and cluster (right). **b**, Average proportions of
577 lung NK cells in each cluster from PBS- or IL-33-treated mice. **c**, Volcano plot of a differential expression analysis comparing IL-33- and PBS-
578 treated NK cells. Red indicates significantly differentially expressed genes (FDR < 0.05). *Ifng* (not significant, blue) and *Gzmb* (significant, dark
579 red) are labelled. **d,e**, Bulk-RNA-seq analysis of sorted lung NK cells from PBS or IL-33-treated WT mice. Expression of NK cell consensus,
580 effector, and both activating and inhibitory receptor transcripts (manually curated) are shown as a heatmap of log₂-transformed normalized read
581 counts of individual genes at the indicated time-points (**d**), or grouped by category for day 3 (z-scaled expression values for genes within the 4
582 gene lists) (**e**). Each point represents the expression value obtained by one replicate for a given gene at a given time point.

583

584 Box plots represent mean (black line), first and third quartiles (box) and range within 1.5 times the interquartile range from the box (whiskers).

585

586 **Figure 7 Activated ILC2 suppress NK cells via an eosinophil-mediated metabolic mechanism**

587

588 **a**, WT mice were treated with IL-33 or PBS on day 0 and 1 and sacrificed on day 3, followed by intracellular detection of phospho-S6 (P-S6)-
589 positive lung NK cells after culture in media ± PI. **b,c**, Mice of the indicated genotypes were treated as in (a) with Asp or PBS, followed by
590 intracellular detection of P-S6 in lung NK cells (**b**, representative data; **c**, MFI, n = 5,5,4,4). **d**, WT mice were treated with PBS or IL-33 on day 0
591 and 1, and anti-IL-5 or control antibody on day -6, -3 and -1 followed by quantification of P-S6⁺ lung NK cells on day 3 (n = 3). **e,f**, Lung cells
592 from WT mice treated as in (a) were: (**e**) cultured for 18 hrs, followed by quantification of glucose (Glu) or lactate (Lac) in the media by NMR (n
593 = 1,3,3), or (**f**) quantification of *ex vivo* 2-NBDG uptake by lung eosinophils. **g**, Lung cells from WT mice treated as in (d) were cultured
594 for 18 hrs, followed by quantification of glucose (Glu) or lactate (Lac) in the media by NMR (n = 5). **h,i**, *Il7ra*^{Cre/+}*Rora*^{fl/fl} or WT mice were treated
595 intranasally with PBS or IL-33 on day 0 and 1, followed by [U-¹³C]glucose infusion and mass spectrometry imaging (MSI) on day 3. H&E and
596 corresponding MSI analysis of [U-¹³C]lactate over [U-¹³C]glucose ratio (pixel per pixel) as shown by heatmap (**h**), and mean relative
597 abundances (**i**, n = 4). **j,k**, Lung cells from WT mice treated as in (a) were assessed for NK cell expression of IFN γ and Gzmb (**j**, n = 6), or P-S6
598 (**k**, n = 7) after cultured (with PI) for 3 hours in normal (Ctrl), no-glucose (-Glu) or high-glucose (+Glu) media. **l**, Lung homogenates were
599 cultured (with PI) for 3 hours, after which NK cells were isolated and assessed for ECAR after addition of glucose, oligomycin, and 2DG (n = 5).
600 **m**, GSEA of PBS and IL-33-treated lung NK cell bulk-RNAseq data (day 3). Normalised enrichment score (NES) and false discovery rate (FDR)
601 shown for each plot. **n**, Lung cells from WT mice treated as in (a) were cultured (with PI) for 3 hours in normal (Ctrl), acidified media (AM), or
602 15 mM lactic acid containing media (+Lac) and assessed for NK cell expression of IFN γ (n = 9,9,9,9,6,6) and Gzmb (n = 3,3,6,6,6,6).

603

604 Bar graphs indicate mean (\pm SEM) and show combined data of two (c, g, i, n) or three (j, k) independent experiments. Data representative of
605 two (b, d, f, h, l, m) or three (a, e) independent experiments. Statistical analyses were calculated using one-way ANOVA with ns = not
606 significant, **** = $p \leq 0.0001$.

607

608 **Figure 8 Therapeutic targeting of the ILC2-eosinophil axis restores NK cell-mediated tumor control**

609

610 **a**, WT mice were treated intranasally with PBS or Asp on day 0 and 1, and IL-33R-Fc or control on day -1 and 1 followed by quantification of
611 IFN γ ⁺ lung NK cells and eosinophilia on day 3 (n = 10). **b-d**, WT mice were treated as indicated (**b**), and lung metastases were quantified by
612 visual examination on day 21 in: (**c**) Asp- or PBS-treated mice (n = 5), or (**d**) IL-33 or PBS-treated mice (n = 5). **e**, BALB/c mice were
613 orthotopically implanted with 4T1 breast cancer cells on day 0, and received treatment with anti-IL-5 or control antibody (days -6, -3, 0, 7 and
614 14), and Asp or PBS intranasally (day 7 and 14), followed by sacrifice on day 21 and visual quantification of lung metastases, and
615 measurement of primary tumour weight (n = 10). **f**, BALB/c mice were orthotopically implanted with 4T1-T breast cancer cells on day 0, and
616 received treatment with anti-IL-5 (days -6, -3, 0, and three times a weeks), or IL33R-Fc or control (day -1 and three times a week) until sacrifice
617 on day 21; the number of lung metastases were measured by visual quantification, and primary tumor weight was measured (n = 10).

618

619 Bar graphs indicate mean (\pm SEM) and shows representative data of two (c) or three (d) independently performed experiments, or combined
620 data of two (a, e and f) independent experiments. Statistical analyses were calculated using one-way ANOVA with **** = $p \leq 0.0001$.

621

622 **Methods**

623 ***In vivo* animal studies**

624 BALB/c, Nod/Scid.*Il2rg*^{-/-} (NSG), C57BL/6J (B6), B6.MMTV-PyMT, B6.*Tyr*^{-/-}, B6.*Il33*^{cit/cit} (*Il33*^{-/-}), B6.*Il7r*^{Cre/+} (provided by Prof. Hans Reimer
625 Rodewald⁵¹), B6.*Il7r*^{Cre/+}*Rora*^{fl/fl}, B6.*Foxp3*^{DTR}, B6.μMT, B6.*Rag2*^{-/-} and B6.*Rag2*^{-/-}*Il7r*^{Cre/+}*Rora*^{fl/fl} mice were maintained in the Cancer Research
626 UK – Cambridge Institute (CRUK-CI) animal facility, under specific-pathogen-free conditions. Mice housed at the CRUK-CI were kept in
627 individually ventilated cages, between 19-23°C with 45-65% humidity and a 12hour dark/light cycle. Some studies were performed at the
628 Medical Research Councils ARES facility (Babraham, UK). Mice were sex and age matched whenever possible, and most mice were used at 8-
629 12 weeks of age. All animal work was conducted under project license PD7484FB9 at the CRUK-CI (with approval from the Cancer Research
630 UK - Cambridge Institute, Animal Welfare Ethical Review Body) or at the Medical Research Councils ARES facility (with approval from
631 Babraham Institute, Animal Welfare Ethical Review Body) all in accordance with Home Office regulation.

632 ***In vivo* experiments**

633 Mice were anesthetized by isoflurane inhalation, followed by the intranasal administration of rmlL-33 (0.2 μg, Biolegend), rmlL-4 (0.5 μg),
634 rmlL-13 (0.5 μg), rmGM-CSF (0.5 μg), rmlL-5 (0.5 μg), LPS (1 μg, Sigma), CpG (10 μg, Invivogen), *Aspergillus* protease allergen (0.01U,
635 Sigma), Ragweed pollen extract (300 μg, Greer) or clodronate liposome (C.L.) (30% C.L./PBS, Liposoma B.V.) in 40 μl of PBS. Diphtheria toxin
636 (10 ng/g, Sigma), IL-33R-Fc (10 mg/kg, AstraZeneca), anti-NK1.1 mAb (50 μg, PK136, BioXcell), anti-CCR2 (20 μg, MC-21, provided by Prof.
637 Matthias Mack⁵²), anti-CCL2 (200 μg, MCP-1, BioXcell), anti-Ly6C/G (200 μg, GR-1, BioXcell), anti-Ly-6G (200 μg, 1A8, BioXcell), anti-CD4
638 (100 μg, GK1.5, BioXcell), anti-IL-10 (300 μg, JES5-2A5, BioXcell), anti-TGF-β (400 μg, 1D11.16.8, BioXcell), anti-IL-5 (100 μg, TRFK5,
639 BioXcell), rat IgG1, κ (BioXcell), rat IgG2a (BioXcell), or rmlL-33 (0.5 μg, Biolegend) was administered by intraperitoneal injection in 100 μl of
640 PBS. A2AR antagonist (20 μg, SCH 58261, Sigma) was administered in DMSO/PBS (v/v).

641

642 **Tumor cells and experimental lung metastasis models**

643 All cell lines used in this study tested negative for Mycoplasma, and were authenticated by STR profiling. B16.F10 (Dr. Jacqueline Shields),
644 B16.F10-mCherry, LL/2 (Dr. Maïke de la Roche), B16.F10-Akaluc, as well as 4T1 (Prof. Greg Hannon) and 4T1-T (Prof. Greg Hannon⁵³) tumor
645 cells were grown in Dulbecco's Modified Eagle's Medium with 10% FBS. Tumor cells were detached using 0.05% Trypsin-EDTA (Gibco) and
646 washed twice in PBS before injection. 1×10^5 B16.F10, 4T1, or 4T1-T, and 2×10^6 LL/2 were used for i.v. injection, unless otherwise stated. All
647 orthotopic injections were performed using 1×10^5 4T1 or 3×10^4 4T1-T mouse mammary tumor cells re-suspended in 30 μ l of PBS. For the
648 early seeding studies 1×10^5 B16.F10-mCherry cells were injected i.v. and lungs collected 24 hours post injection. In the autochthonous breast
649 cancer model twelve-week-old female B6.MMTV-PyMT mice were randomized and treated intranasally with IL-33, Asp or PBS once a week
650 and sacrificed at 20 weeks of age, followed by visual quantification of lung metastases, and weighing of primary tumours. Tumors on the lung
651 surface were quantified by counting the metastatic foci under a dissection microscope, after which lungs were collected for further processing.
652 For survival studies mice were treated as described in the figures and injected with B16-F10 tumor cells at day 0, mice were monitored daily
653 and were sacrificed when reaching the humane endpoint.

654

655 **Live imaging studies**

656 Third generation lentiviral particles were produced by transient co-transfection of 293FT cells with Akaluc⁵⁴-plasmid (Kindly provided by Prof.
657 Greg Hannon) and the three packaging constructs pMDL, CMV-Rev, and VSV-G. Lentivirus containing particles were concentrated on
658 Centricon Plus-70 filters (Millipore) and B16.F10 cells were infected with concentrated lentivirus in the presence of 8 mg/ml polybrene, and
659 selected 3 days after infection with neomycin (Geneticin 1 mg/ml, Invitrogen). IVIS bioluminescent imaging was performed by *in vitro* exposure
660 of B16.F10-Akaluc cells to 250 μ M Akalumine substrate for 30 minutes at 37 °C in a humidified, 5% CO₂ incubator. The cells were washed with
661 PBS twice and 1×10^5 cells were injected i.v. into B6.*Tyr*^{-/-} mice and imaging was performed 2, 10, and 30 min after. Total photon emission from
662 the thorax of each mouse was quantified with the LivingImage software package (Xenogen).

663

664 **Single cell preparation**

665 Cell suspensions were prepared from lung by mechanical dissociation, followed by digest in 5 ml of RPMI-1640 containing collagenase I (500
666 U/ml) and DNase I (0.2 mg/ml) for 45 minutes at 37 °C on a shaker (220 rpm), followed by filtration through a 70 µm strainer and 25% Percoll
667 gradient enrichment of leukocytes, and red blood cell (RBC) lysis. Tumor cell were recovered without Percoll enrichment. Blood cells were
668 lysed in 5 ml RBC lysis buffer 3 times for 5 minutes and spleens were strained through a 70 µm filter in RPMI-1640 before lysing erythrocytes
669 with RBC lysis buffer for 5 minutes. Single-cells were re-stimulated and stained for surface and intracellular markers (*see flow cytometry*).

670

671 **Primary cell culture**

672 Mouse primary cells were cultured in RPMI-1640 supplemented with 10% FCS, 100 U/ml penicillin (Invitrogen), and 100 µg/ml streptomycin
673 (Invitrogen). Cells were cultured at 37 °C in a humidified, 5% CO₂ incubator.

674

675 **NK cell isolation and co-culture**

676 Single cell suspension from PBS or IL-33-sensitised lung were used to isolate NK cells by magnetic bead negative selection strategy (EasySep,
677 StemCell), according to manufacturer's protocol. NK cell purity was assessed by flow cytometry and cells were used when purity exceeded
678 90%. Purified NK cells were cultured overnight, alone or with CFSE-labelled PBS or IL-33 lung single cell suspensions in different ratio's.
679 Alternatively, NK cells were co-cultured with sort purified ILC2 cells overnight in equal concentrations.

680

681 **Eosinophil culture and adoptive transfer**

682 Bone marrow derived eosinophils were cultured as described before⁵⁵. Briefly, bone marrow derived progenitor cells were differentiated for 4
683 days in IMDM with GlutaMAX-1 (Gibco) with 10% FBS, 100 U/ml penicillin (Invitrogen), and 100 µg/ml streptomycin (Invitrogen) supplemented
684 with 100 ng/ml Stem Cell Factor (Pepro Tech) and 100 ng/ml Flt3 ligand (Pepro Tech) at a concentration of 1×10⁶/ml. Thereafter, expanded

685 progenitor cells were differentiated into eosinophils using 10 ng/ml recombinant mouse IL-5 (Pepro Tech) for 10 days and derived eosinophils
686 were subsequently co-cultured with purified NK cells at different ratio's or adoptively transferred into recipient mice (3×10^6 /mouse).

687

688 **Glucose and lactate cultures**

689 For *in vitro* glucose uptake experiments, mouse primary cells were cultured in glucose-free RPMI-1640 (Gibco) supplemented with 10% FCS,
690 and 2-NBDG (50 μ M, Thermo Fisher). Cells were cultured for 1 hour at 37 °C in a humidified, 5% CO₂ incubator, followed by harvest,
691 processing and flow cytometry analysis at 4 °C. For glucose-deficient or glucose-high experiments, mouse primary lung cells were cultured in
692 glucose-free RPMI-1640 (Gibco) supplemented with 10% FCS, +/- glucose (2.0 or 4.5 mM), 100 U/ml penicillin (Invitrogen), and 100 μ g/ml
693 streptomycin (Invitrogen). Cells were cultured for 3 hours at 37 °C in a humidified, 5% CO₂ incubator, followed by harvest, processing and flow
694 cytometry analysis at 4 °C. For lactic acid experiments, mouse primary lung cells were cultured in RPMI-1640 supplemented with 10% FCS,
695 100 U/ml penicillin (Invitrogen), 100 μ g/ml streptomycin (Invitrogen), and either: a) lactic acid (15 mM, pH 6.4 Sigma), b) HCl (pH 6.4), or c)
696 normal pH (7.4). Cells were cultured for 3 hours at 37 °C in a humidified, 5% CO₂ incubator, followed by harvest, processing and flow cytometry
697 analysis at 4 °C. For intracellular cytokine detection, PMA + ionomycin and protein transport inhibitor (Thermo Fisher) was added during the 3-
698 hour culture.

699

700 **Sample preparation and 1H NMR analysis**

701 For metabolic profiling of lung cultures, WT mice were treated with IL-33 or PBS on day 0 and 1, followed by culture of 1×10^6 cells (whole lung)
702 for 18 hours in 200 μ L of RPMI-1640 supplemented with 10% FCS, 100 U/ml penicillin (Invitrogen), and 100 μ g/ml streptomycin (Invitrogen).
703 Cells were cultured at 37 °C in a humidified, 5% CO₂ incubator. Three technical replicates were set up for each mouse, and combined (600 μ L)
704 for NMR analysis. 590 μ L of sample was placed in a 5 mm Wilmad standard NMR tube and 10 μ L of 60 mM TSP was added as the chemical
705 shift and internal quantitation standard. 1H NMR spectra were acquired on a 600 MHz Bruker Avance NMR spectrometer using a water pre-
706 saturation sequence with 1024 averages, 5sec repetition time, 2.28sec acquisition time (TR=7.28sec) and 32K time domain data points. The

707 time domain data were pre-processed by 0.5 Hz line broadening, Fourier transformation, zero and first order phase correction. Chemical shifts
708 were assigned from the human metabolomic data base (HMDB; <http://www.hmdb.ca/>) and also from our own 2D-NMR spectral (COSY and
709 TOCSY) data. The absolute metabolite concentrations of the media were estimated using the NMR suite 8.3 (Chenomx® Software package)
710 using the internal standard TSP concentration.

711

712 **Cytotoxicity assays**

713 To determine their *ex vivo* cytotoxic capacity we purified PBS- or IL33-exposed NK cells from mouse lungs using a magnetic bead negative
714 selection strategy (EasySep, StemCell), according to manufacturer's protocol. Purified NK cells (>85%) were subsequently CFSE-stained (5
715 μ M final concentration in PBS) and co-cultured with >1.5 weeks passaged YAC-1 cells at 10:1 (NK/YAC-1) ratio in RPMI-1640. Addition of
716 Annexin V Red (Essen Bioscience) allowed us to follow target cell killing using the Incucyte platform (Incucyte software v2018A, Essen
717 Bioscience).

718

719 **Flow cytometry**

720 Single cells were incubated with anti-mouse CD16/32 (Thermo Fisher) to block Fc receptors and stained as indicated. Lineage cocktail
721 contained (\pm CD3 (145-2C11), \pm NK1.1 (PK136), TCR β , CD5 (53-7.3), CD19 (1D3), CD11b (M1/70), CD11c (N418), Fc ϵ R1 α (MAR-1), F4/80
722 (BM8), Ly-6C/G (Rb6-8C5), and Ter119 (TER-119) all on eFluor450 (eBioscience)). For intracellular staining we used the Foxp3/Transcription
723 Factor Kit (Thermo Fisher), or Cytofix/Cytoperm Kit (BD Bioscience) as per manufacturer's instructions. For intracellular cytokine detection,
724 single cells were stimulated with PMA (60 ng/ml) and ionomycin (500ng/ml) plus 1 \times protein transport inhibitor (Thermo Fisher), 1 \times cytokine
725 stimulation cocktail (Thermo Fisher), or plate bound anti-NK1.1 mAb (10-30 μ g/ml, BioXcell), or recombinant IL-12 (20 ng/ml) and IL-18 (5
726 ng/ml) in culture media (RPMI-1640, 10% FCS) at 37 °C for 3 hours before staining. Data was acquired on a BD Fortessa or Symphony
727 instrument, cells were quantified using CountBright beads. Data was analysed using FlowJo X (Tree Star).

728

729 B220 (RA3-6B2, Life Technologies, APC.eFluor780), CD3e (145-2C11, eBioscience, PE.Cy7 and eFluor450) (25-0031-83, 4304567), CD4 (RM4-5,
730 eBioscience, AF700), CD5 (53-7.3, eBioscience, eFluor450), CD8 (53-6.7, eBioscience, PerCP.eFluor710 and SB645), CD11b (M1/70, eBioscience,
731 eFluor450, APC.eFluor780, and BV785), CD11c (N418, eBioscience, eFluor450 and AF700), CD16/32 (93, Biolegend), CD19 (1D3, eBioscience,
732 eFluor450), CD31 (390, Biolegend, BV605), CD45 (30-F11, Biolegend, BV510), CD49b (HMA2, BD, BV650), CD64 (X54-5/7.1 Biolegend, BV711),
733 CD127 (SB/199, BD, PE.CF594), CD172a (P84, Biolegend, AF488), EpCam (G8.8, Biolegend, BV711), FcεR1a (MAR-1, eBioscience, eFluor450
734 and PerCP.eFluor710), Fixable Viability Dye (eBioscience, UV455), F4/80 (BM8, eBioscience, eFluor450 and APC.eFluor780), Foxp3 (FJK-16s,
735 eBioscience, AF488), GATA3 (TWAJ, eBioscience, eFluor660), Granzyme B (NGZB, eBioscience, PerCP.eFluor710), I-A/I-E (CI2G9, BD, BUV395),
736 ICOS (7E.17G9, eBioscience, PE), IFNγ (XMG1.2, Biolegend, BV786), IL-5 (TRFK5, BD, APC), Ki67 (CIB56, BD, BV786), Ly-6C/G (Rb6-8C5,
737 eBioscience, eFluor450), Ly-6G (1A8-Ly6g, eBioscience, PE.eFluor610), Ly-6C (HK1.4, eBioscience, PE.Cy7), NK1.1 (PK136, BD, BUV395 and
738 eBioscience, eFluor450), RELMα (DS8RELM, Invitrogen, APC), Phospho-S6 (cupk43k, eBioscience, PE), Podoplanin (8.1.1, Biolegend, PE.Cy7),
739 Roryt (Q31.378, eBioscience, PerCP.eFluor710), SiglecF (1RNM44N, eBioscience, SB600), ST2 (RMST2-2, eBioscience, PE), Ter119 (TER-119,
740 eBioscience, eFluor450).

741

742 **Metabolic analysis**

743 ECAR was measured using the Seahorse XF96 Extracellular Flux Analyzer (Agilent Technologies). PBS or IL-33 lung homogenates were
744 stimulated 3 hours with PMA (60 ng/ml) and ionomycin (500ng/ml) at 37°C in a 5% CO₂ incubator. Cells were collected and NK cells were
745 purified by magnetic bead negative selection strategy (EasySep, StemCell), according to manufacturer's protocol. Cells were suspended in XF
746 Base Minimal RPMI (pH7.4) with L-Glutamine (2 mM), and were plated into a culture microplate (5x10⁵ cells/well; Agilent Technologies). Prior
747 to real-time measurement of the ECAR, Glucose (20 mM), oligomycin (1,5 μM), and 2DG (50 mM) were added.

748

749 **Mass Spectrometry Imaging (MSI) Sample Preparation, Acquisition and Data Analysis**

750 Mice were anesthetized with isoflurane, maintained at 37°C and administered with [U-¹³C]glucose (Cambridge Isotope Laboratories, Andover,
751 MA) as a bolus at 0.4 mg/g, followed by continuous infusion of 0.012 mg/g/min at 300 µL/h for 120 min⁵⁶. The lungs were rapidly removed and
752 snap frozen in dry ice chilled isopentane and stored at -80°C until sectioning. Lungs were sectioned to 10 µm thickness using a CM3050 cryo-
753 microtome (Leica Biosystems, Nussloch, Germany) and thaw-mounted onto Superfrost slides (Fisher Scientific, Loughborough, UK) for
754 desorption electrospray ionization (DESI) MSI and histological examination. Tissue section slides were vacuum packed and stored at -80°C
755 until analysis.

756

757 DESI MSI was carried out using an automated 2D DESI source (Prosolia Inc, Indianapolis, IN, USA) with home-built sprayer assembly⁵⁷
758 mounted to a Q-Exactive FTMS instrument (Thermo Scientific, Bremen, Germany). Analyzes were performed at spatial resolutions between 40
759 µm in negative ion mode and mass spectra were collected in the mass range of 80–900 Da with mass resolving power set to 70000 at *m/z* 200
760 and an S-Lens setting of 100. Methanol/water (95:5 v/v) was used as the electrospray solvent at a flow rate of 1.0 µL/min and a spray voltage
761 of -4.5kV. Distance between DESI sprayer to MS inlet was 7mm, while distance between sprayer tip to sample surface was 1.5mm at an angle
762 of 75°. Nitrogen N4.8 was used as nebulizing gas at a pressure of 6.5 bar. Omnispray 2D (Prosolia, Indianapolis, USA) and Xcalibur (Thermo
763 Fisher Scientific Inc) software were used for MS data acquisition. Individual line scans were converted into centroided. mzML format using
764 MSConvert (ProteoWizard toolbox version 3.0.4043) and subsequently into .imzML using imzML converter v1.3. Hematoxylin and eosin (H&E)
765 staining was performed post analysis on same lung sections and the stained sections were imaged at 40x with Aperio CS2 digital pathology
766 scanner (Aperio Tech., Oxford, UK), and visualized with ImageScope software (Aperio Tech.).

767

768 Mass Imaging data were visualized and analyzed using SCiLS Lab MVS 2019b software (SCiLS GmbH, Bremen, Germany). MS images were
769 normalized to RMS (Root Mean Square) to compensate for signal instabilities and allow comparison between multiple experiments. Exact mass
770 measurements only were used for metabolite identification with mass deviations <8ppm (see below). For labelled metabolites no mass
771 interferences were found on non-infused samples MS images.

772

773 (Metabolite; Ion Cluster; m/z theoretical; m/z measures; error): Lactate; [M-H]⁻; 89.024418; 89.02386; 6.3, [U-¹³C]Lactate; [M-H]⁻; 92.033379;
774 92.03269; 7.5, Glucose; [M+Cl]⁻; 215.032789; 215.03241; 1.8, [U-¹³C]Glucose; [M+Cl]⁻; 221.05291; 221.05359; 3.1.

775

776 A bisecting k-means algorithm using a weak pixel denoising and distance correlation as parameters were applied to provide unsupervised
777 clustering of MS images to create regions corresponding to each lung sample. Then, the mean relative abundance of each molecular species
778 for pixels of the image was extracted from each sample and expressed in arbitrary unit (a.u.).

779

780 **Histology**

781 Lung lobes were fixed in 10% neutral buffered formalin in PBS for 24 hours, followed by transfer to 70% Ethanol in PBS for another 24 hours
782 and embedded into paraffin. 3 µm sections were cut and stained with Ki-67. The CRUK-CI Histology Core performed tissue embedding,
783 sectioning and staining. Image quantification was performed using the HALO software (HALO, Indica labs).

784

785 **Bulk-RNA-seq**

786 Mouse lungs were dissected and made to single cell suspension as described above, followed by staining with with anti-mouse CD16/32
787 (Thermo Fisher) to block Fc receptors, Lineage cocktail (anti-CD5, CD19, CD11c, FcεR1α, F4/80, Ly-6C/G, and Ter119) eFl450, anti-CD45
788 BV510, anti-CD49b BV605, anti-NK1.1 BUV395, anti-CD3 PE-Cy7, anti-B220 APC-eFl780, and anti-CD4 AF700. Dead cells were excluded by
789 DAPI staining, followed by electronic gating of live CD45⁺Lineage^{int}CD3⁻CD4⁻B220⁻NK1.1⁺CD49b⁺ NK cells which were purified by FACS (BD
790 Aria II, Becton Dickinson). Purity checks were performed after each sort, with all used samples being >95% pure.

791

792 1 µg of total RNA was used as input material for library preparation. The NEBNext Poly(A) mRNA magnetic Isolation Module (NEB) was used
793 to isolate poly(A) RNAs. Libraries were generated with the NEBNext Ultra Directional RNA Library Prep kit for Illumina (NEB) according to
794 manufacturer's instructions. The pooled libraries were quantified with KAPA Library Quantification Kit for Illumina (Kapa Biosystems) and
795 sequenced (single end 50nt) on an Illumina HiSeq 4000 (Illumina).

796

797 **Bulk RNA-seq analysis**

798 Sequence data were aligned to the GRCm38 mouse reference genome using STAR (v2.7.3)⁵⁸. Quality control metrics were computed using
799 Picard CollectAlignmentStatistics and CollectRnaSeqMetrics (<https://broadinstitute.github.io/picard>). Assignment and quantification of reads to
800 transcripts from Ensembl release 98 (<https://www.ensembl.org>) were performed using featureCounts from the subread package (v1.5.2)⁵⁹.
801 DESeq2⁶⁰ was used to estimate size factors for normalization, estimate dispersions, fit a negative binomial GLM and calculate Wald statistics
802 for differential expression between sample groups. Gene set enrichment analysis was performed using GSEA software and gene set collection
803 7.1 (Hallmark signatures). (<http://software.broadinstitute.org/gsea/index.jsp>).

804

805 A power calculation was carried out with PROPER⁶¹ using estimates of the variance from the first bulk RNA-seq analysis in which there were 3
806 replicates for each group. The second RNA-seq analysis had 7 replicate samples taken from mice on day 2 following treatment with PBS and
807 IL-33. The data for one replicate in the IL-33 group failed QC based on depth of coverage and clustering in a principal components analysis and
808 was discarded.

809

810 **Single-cell RNAseq processing and quality control**

811 WT mouse lung NK cell FACS purification was performed identical to bulk-RNA-seq experiments. Mapping and counting of 10x Genomics
812 scRNA-seq reads was performed using Cell Ranger (v 3.1.0) without filtering droplets. Reads with swapped barcodes and empty droplets were

813 identified for filtering using the swappedDrops and emptyDrops functions from the DropletUtils (v1.4.3) Bioconductor package^{62, 63}. Data were
814 further processed using scran (v1.12.1), scater (v1.12.2) and SingleCellExperiment (v1.6.0) Bioconductor packages^{64, 65}. Poor quality cells with
815 \log_{10} total UMIs less than 3 median absolute deviations (MADs) from the median, total genes detected less than 3 MADs from the median, or
816 \log_{10} ratio of mitochondrial to non-mitochondrial gene UMIs deviating more than 3 MADs from the median were removed. Normalization was
817 carried out by deconvolving cell pools as implemented in the computeSumFactors function from the scran Bioconductor package⁶⁶. To remove
818 contaminating myeloid cells, we first identified lung myeloid- and NK-cell specific genes using the following sources: population comparison of
819 splenic NK cells versus lung alveolar macrophages from the ImmGen RNA-seq database⁶⁷ (analysis specified genes always expressed in one
820 population and never in the other; selected top 10 with highest expression); alternatively activated macrophage markers from Holtzman et al.⁶⁸;
821 alveolar macrophage genes from Misharin et al.⁶⁹; and NK cell genes from Crinier et al.⁷⁰. Expression of myeloid-specific and NK cell specific
822 genes was largely mutually exclusive. Cells that expressed more myeloid-specific than NK cell-specific genes were classified as contaminating
823 cells and were removed.

824

825 **Single-cell RNAseq analysis**

826 Clustering was performed by the Louvain method on a shared nearest neighbours graph as implemented in the scran and igraph (v1.2.4.1)
827 packages. Marker genes for each cluster were identified using the findMarkers function from scran, selecting genes differentially expressed
828 compared to all other clusters. Cell-specific scores for cell cycle phases were calculated using the CellCycleScoring function from the Seurat
829 (v3.1.1) package⁷¹ after converting supplied human phase-associated genes to their murine orthologues using BioMart (biomaRt v2.40.5).
830 Cluster abundances were modelled using a quasi-likelihood negative binomial GLM and differential abundances between PBS and IL-33-
831 treated samples tested with empirical Bayes quasi-likelihood F-tests, as implemented in the edgeR (v3.26.8) Bioconductor package⁷².
832 Abundance analyses were performed by normalizing based on cell number and without estimating a trend on the dispersion due to the small
833 number of clusters. After filtering for genes detected in at least 1% of cells, differential expression analysis controlling for cluster abundances
834 and cluster-specific treatment effects was also performed through the edgeR negative binomial GLM framework⁷³, modelling gene expression
835 as a function of sample, cluster, and cluster-sample interactions. A likelihood ratio test was performed contrasting IL-33-treated sample

836 coefficients with PBS-treated sample coefficients. Analysis code for scRNA-seq is available at
837 (<https://github.com/MarioniLab/scRNAseqLungNKcells>).

838

839 **Statistics**

840 Analysis for two groups were calculated using unpaired two-tailed Student's t-test, comparisons of more than two groups were calculated using
841 one-way ANOVA with Tukey post-analysis, or Log-rank (Mantel-Cox) test where necessary. Data were analysed using GraphPad Prism 8
842 (GraphPad Software) with $p \leq 0.05$ being considered significant.

843

844 **DATA AND SOFTWARE AVAILABILITY**

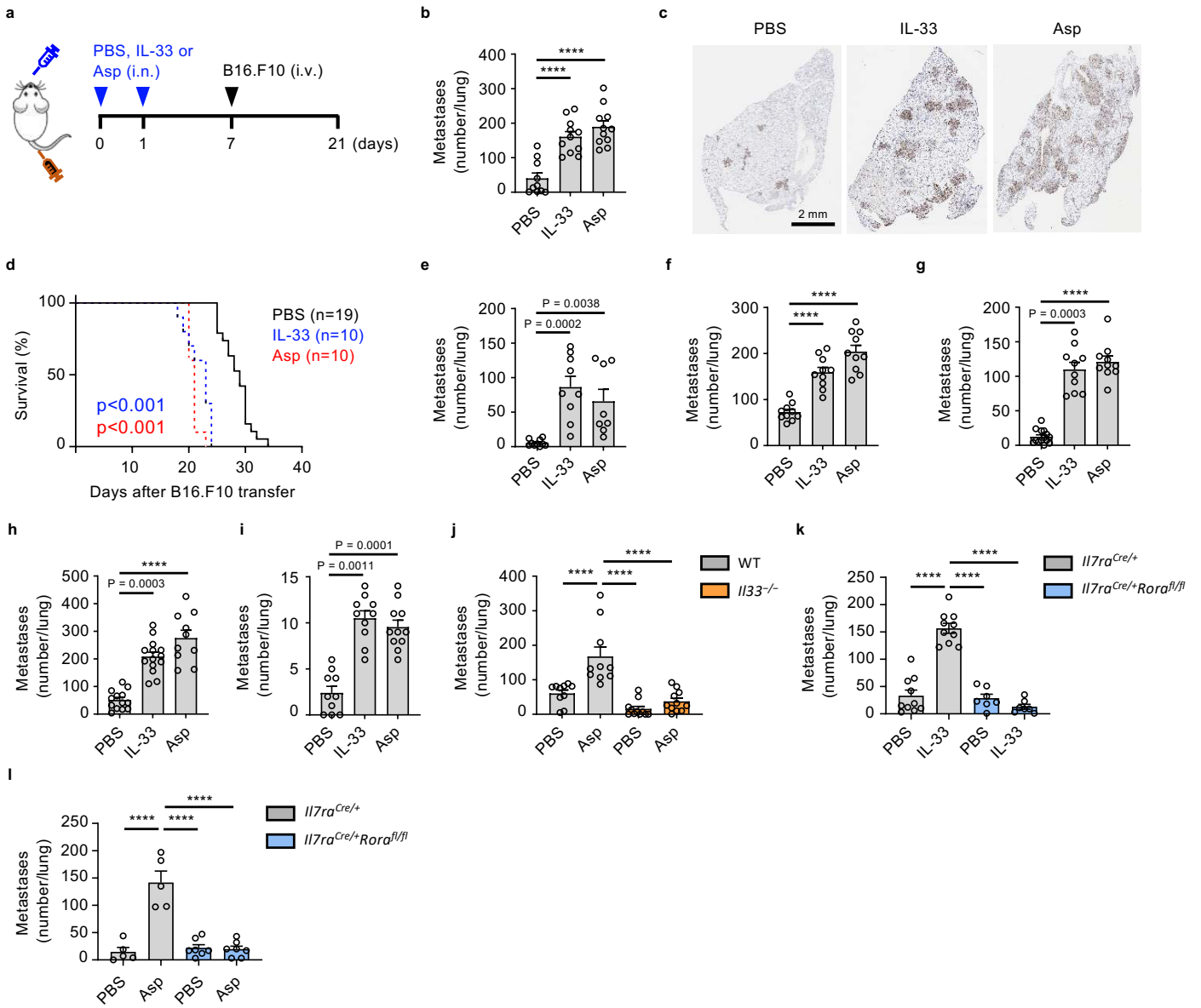
845 Transcriptomic data used in Fig. 6 and Extended Data Fig. 7 are available at the Sequence Read Archive (SRA) under the Bioproject
846 PRJNA637311 : Lung NK cell transcriptomic. Bulk RNAseq data are available with the following BioSample accession numbers:
847 SAMN15099850 (bulk PBS vs IL33) and the following sample names are A1, D1, B2, C2, F2, E1 and H1 for the PBS-treated condition and D2,
848 B1, F1, E2, A2 and G1 for IL33-treated condition; SAMN15099866 (time-course) with the following triplicate sample names E4, A4, C3 (WT
849 PBS day 3), H3, F4, D3 (WT IL33 day 3), C4, G4, A3 (WT IL33 day 7), B4, E3, G3 (WT IL33 day 14) and D4, F3, B3 (IL2KO IL33 day 3).

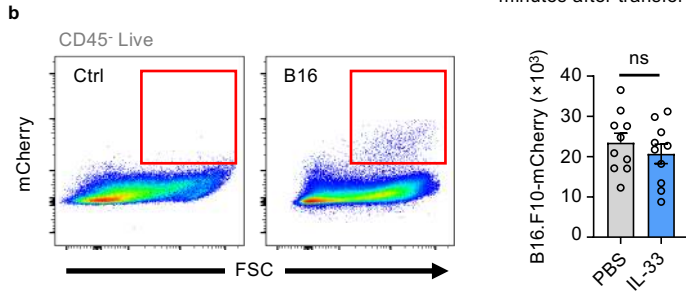
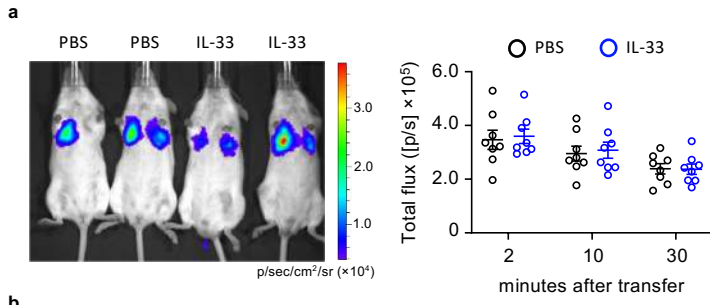
850 **Methods-only References**

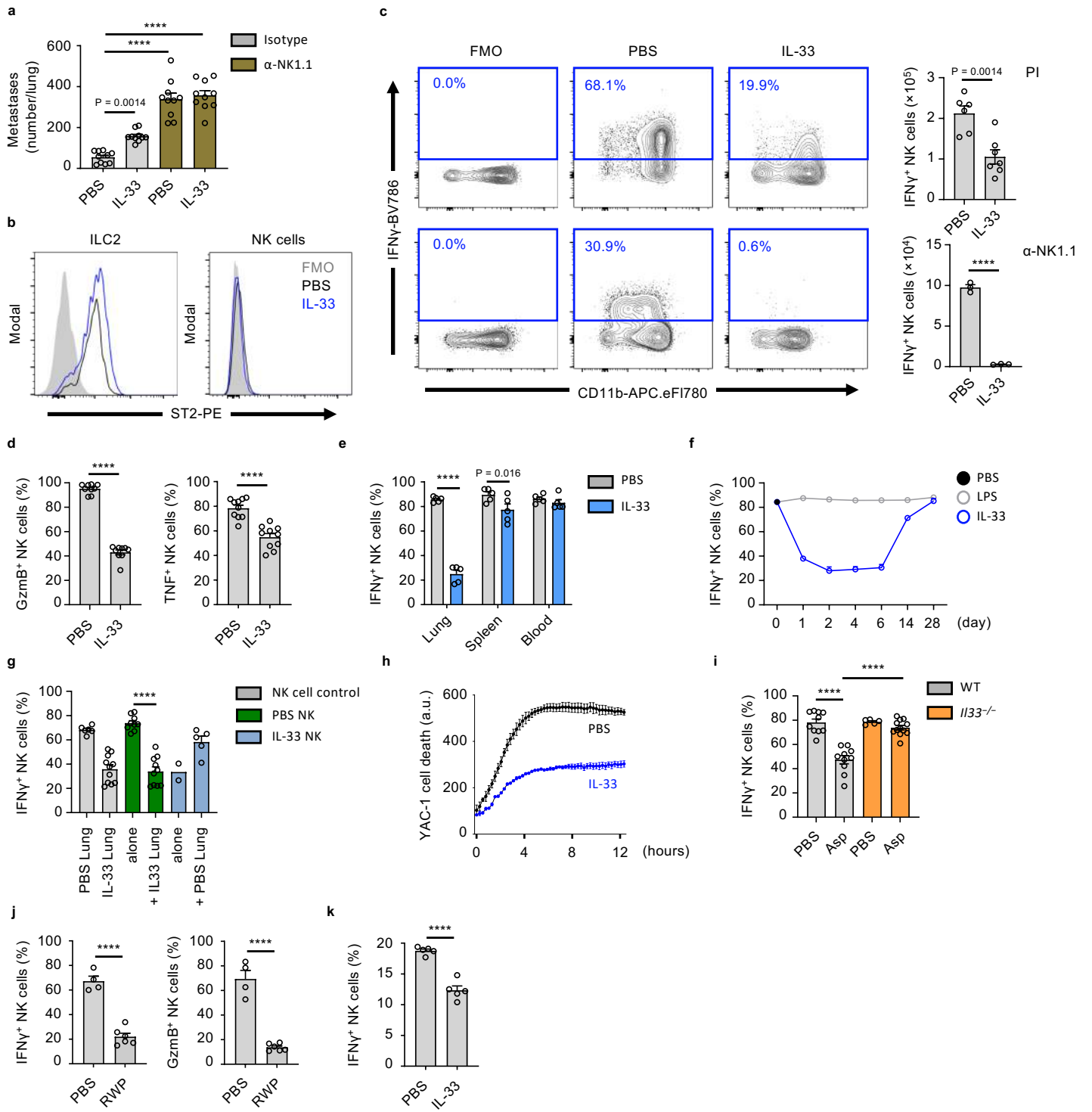
- 851 51. Schlenner, S.M. *et al.* Fate mapping reveals separate origins of T cells and myeloid lineages in the thymus. *Immunity* **32**, 426-436
852 (2010).
853
- 854 52. Mack, M. *et al.* Expression and characterization of the chemokine receptors CCR2 and CCR5 in mice. *J Immunol* **166**, 4697-4704
855 (2001).
856
- 857 53. Wagenblast, E. *et al.* A model of breast cancer heterogeneity reveals vascular mimicry as a driver of metastasis. *Nature* **520**, 358-
858 362 (2015).
859
- 860 54. Iwano, S. *et al.* Single-cell bioluminescence imaging of deep tissue in freely moving animals. *Science* **359**, 935-939 (2018).
861
- 862 55. Lu, T.X. & Rothenberg, M.E. Bone Marrow Derived Eosinophil Cultures. *Bio Protoc* **4** (2014).
863
- 864 56. Marin-Valencia, I. *et al.* Analysis of tumor metabolism reveals mitochondrial glucose oxidation in genetically diverse human
865 glioblastomas in the mouse brain in vivo. *Cell Metab* **15**, 827-837 (2012).
866
- 867 57. Takats, Z., Wiseman, J.M., Gologan, B. & Cooks, R.G. Mass spectrometry sampling under ambient conditions with desorption
868 electrospray ionization. *Science* **306**, 471-473 (2004).
869
- 870 58. Dobin, A. *et al.* STAR: ultrafast universal RNA-seq aligner. *Bioinformatics* **29**, 15-21 (2013).
871
- 872 59. Liao, Y., Smyth, G.K. & Shi, W. featureCounts: an efficient general purpose program for assigning sequence reads to genomic
873 features. *Bioinformatics* **30**, 923-930 (2014).
874
- 875 60. Love, M.I., Huber, W. & Anders, S. Moderated estimation of fold change and dispersion for RNA-seq data with DESeq2. *Genome*
876 *Biol* **15**, 550 (2014).
877
- 878 61. Wu, H., Wang, C. & Wu, Z. PROPER: comprehensive power evaluation for differential expression using RNA-seq. *Bioinformatics*
879 **31**, 233-241 (2015).
880

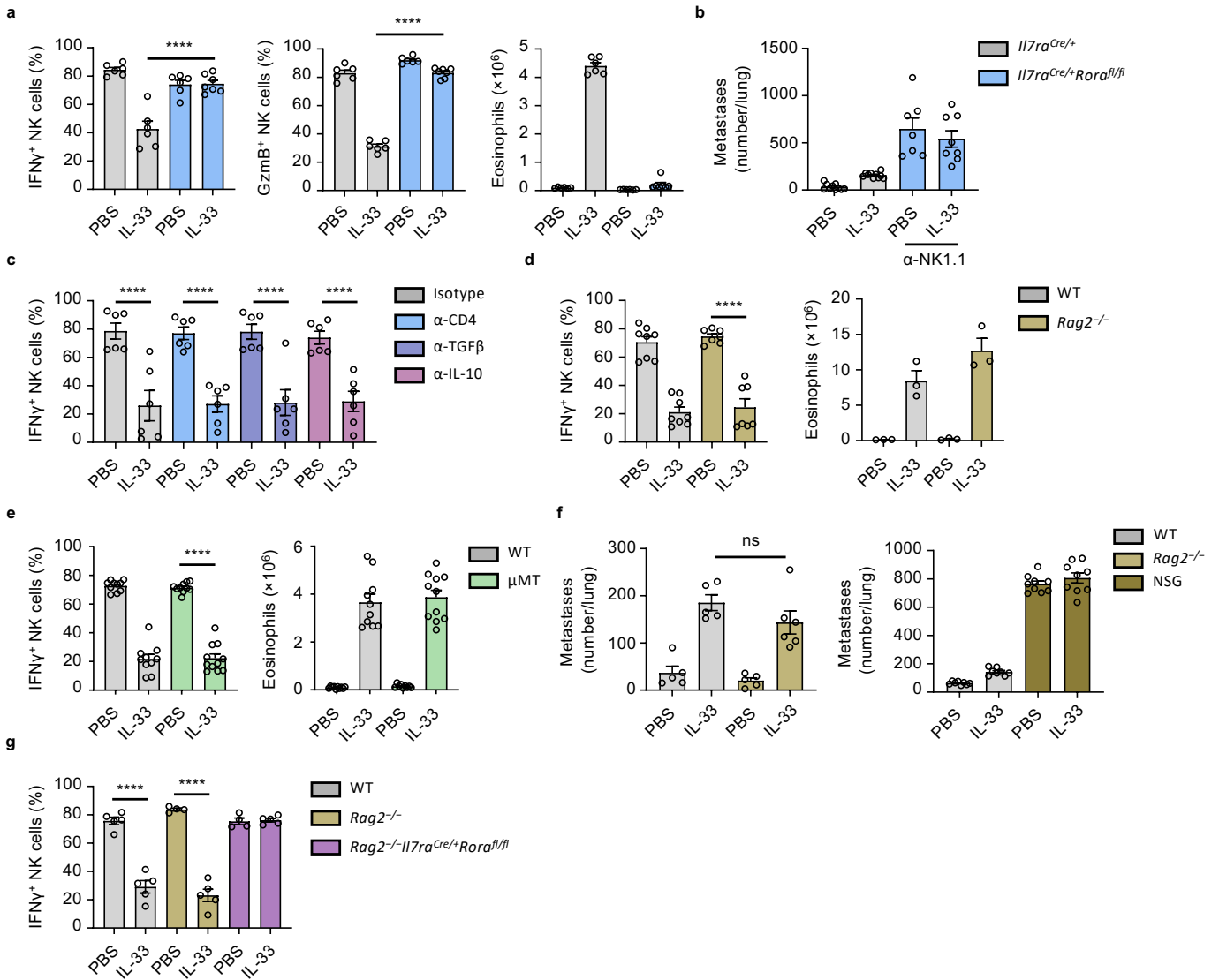
- 881 62. Lun, A.T.L. *et al.* EmptyDrops: distinguishing cells from empty droplets in droplet-based single-cell RNA sequencing data. *Genome*
882 *Biol* **20**, 63 (2019).
883
- 884 63. Griffiths, J.A., Richard, A.C., Bach, K., Lun, A.T.L. & Marioni, J.C. Detection and removal of barcode swapping in single-cell RNA-seq
885 data. *Nat Commun* **9**, 2667 (2018).
886
- 887 64. Lun, A.T., McCarthy, D.J. & Marioni, J.C. A step-by-step workflow for low-level analysis of single-cell RNA-seq data with
888 Bioconductor. *F1000Res* **5**, 2122 (2016).
889
- 890 65. McCarthy, D.J., Campbell, K.R., Lun, A.T. & Wills, Q.F. Scater: pre-processing, quality control, normalization and visualization of
891 single-cell RNA-seq data in R. *Bioinformatics* **33**, 1179-1186 (2017).
892
- 893 66. Lun, A.T., Bach, K. & Marioni, J.C. Pooling across cells to normalize single-cell RNA sequencing data with many zero counts.
894 *Genome Biol* **17**, 75 (2016).
895
- 896 67. Heng, T.S., Painter, M.W. & Immunological Genome Project, C. The Immunological Genome Project: networks of gene expression
897 in immune cells. *Nat Immunol* **9**, 1091-1094 (2008).
898
- 899 68. Holtzman, M.J., Byers, D.E., Alexander-Brett, J. & Wang, X. The role of airway epithelial cells and innate immune cells in chronic
900 respiratory disease. *Nat Rev Immunol* **14**, 686-698 (2014).
901
- 902 69. Misharin, A.V., Morales-Nebreda, L., Mutlu, G.M., Budinger, G.R. & Perlman, H. Flow cytometric analysis of macrophages and
903 dendritic cell subsets in the mouse lung. *Am J Respir Cell Mol Biol* **49**, 503-510 (2013).
904
- 905 70. Crinier, A. *et al.* High-Dimensional Single-Cell Analysis Identifies Organ-Specific Signatures and Conserved NK Cell Subsets in
906 Humans and Mice. *Immunity* **49**, 971-986 e975 (2018).
907
- 908 71. Stuart, T. *et al.* Comprehensive Integration of Single-Cell Data. *Cell* **177**, 1888-1902 e1821 (2019).
909
- 910 72. Lun, A.T., Chen, Y. & Smyth, G.K. It's DE-licious: A Recipe for Differential Expression Analyses of RNA-seq Experiments Using
911 Quasi-Likelihood Methods in edgeR. *Methods Mol Biol* **1418**, 391-416 (2016).
912

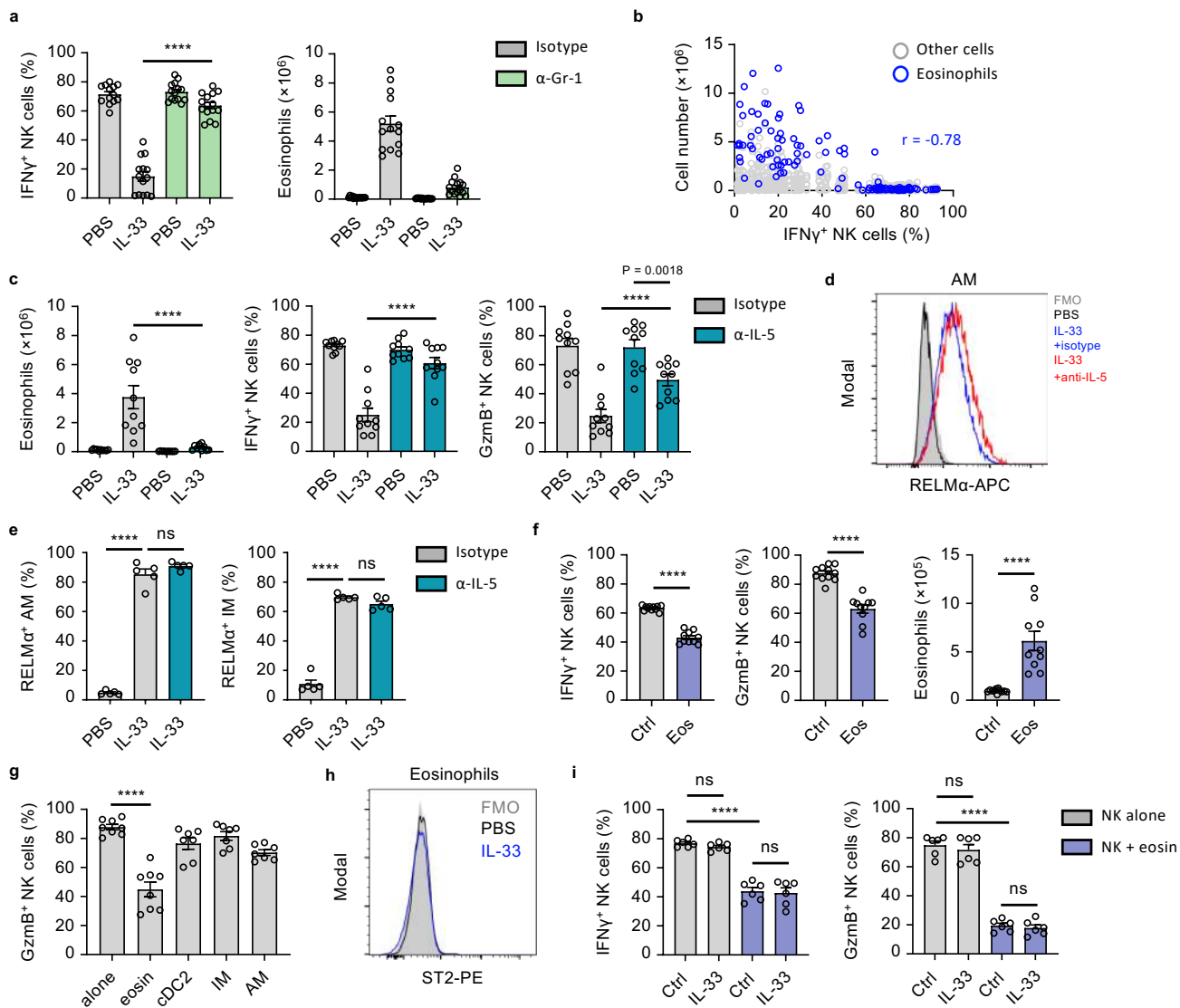
- 913 73. McCarthy, D.J., Chen, Y. & Smyth, G.K. Differential expression analysis of multifactor RNA-Seq experiments with respect to
914 biological variation. *Nucleic Acids Res* **40**, 4288-4297 (2012).
915
916
917

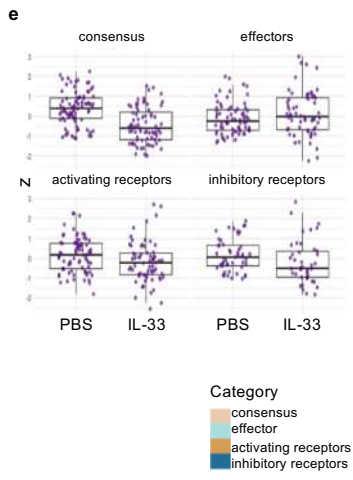
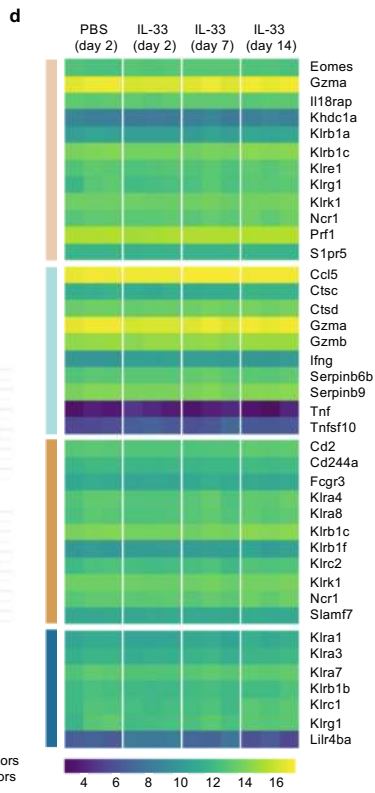
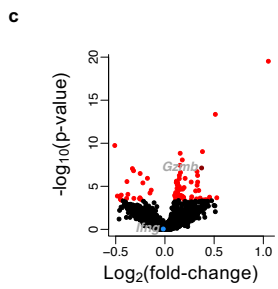
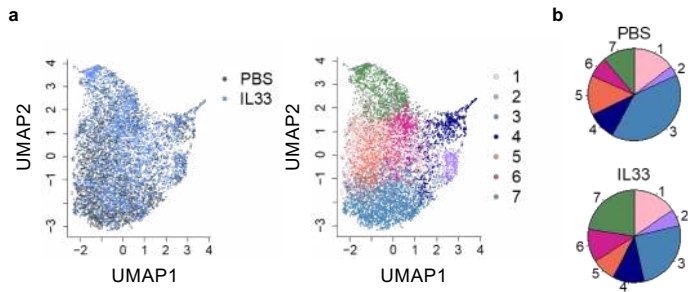


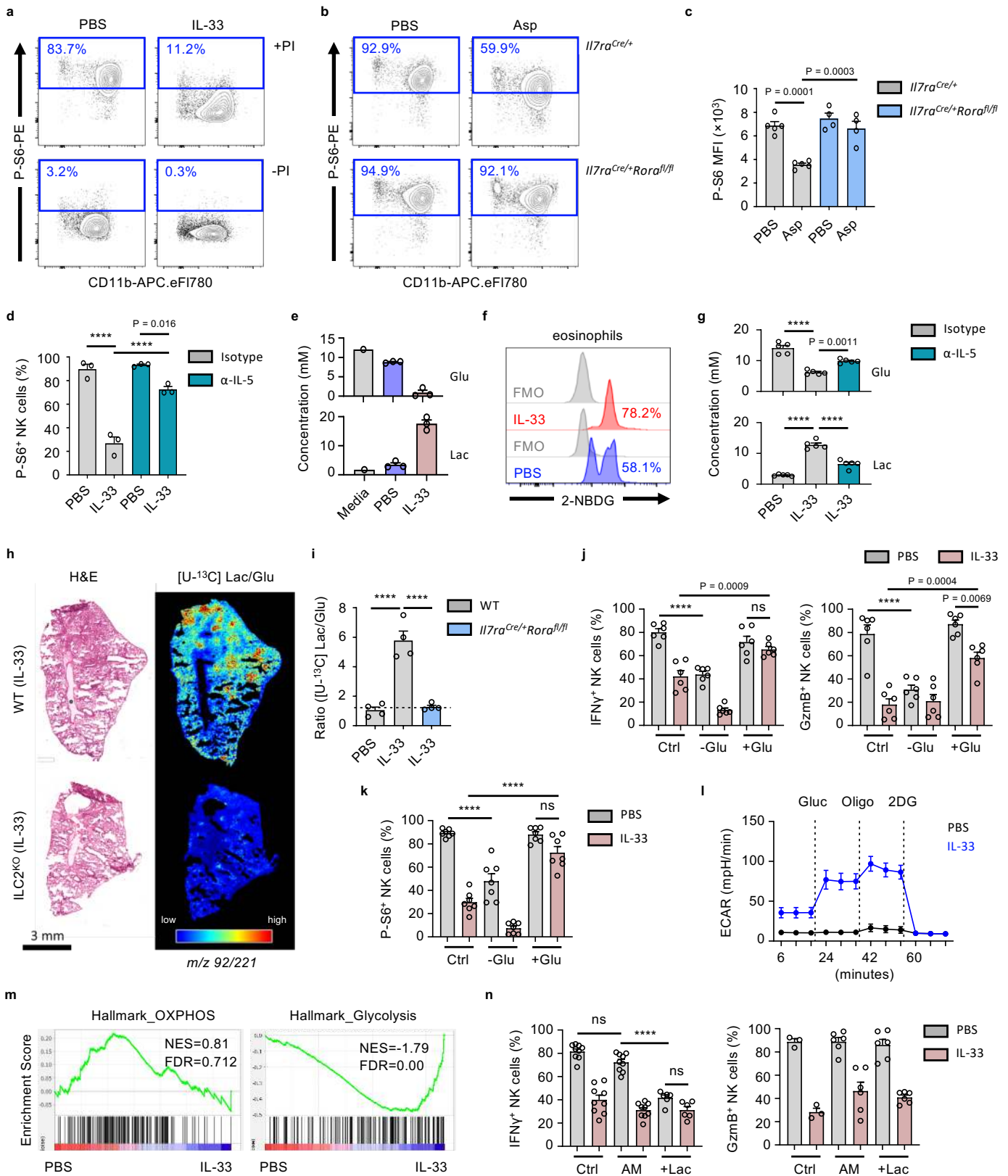


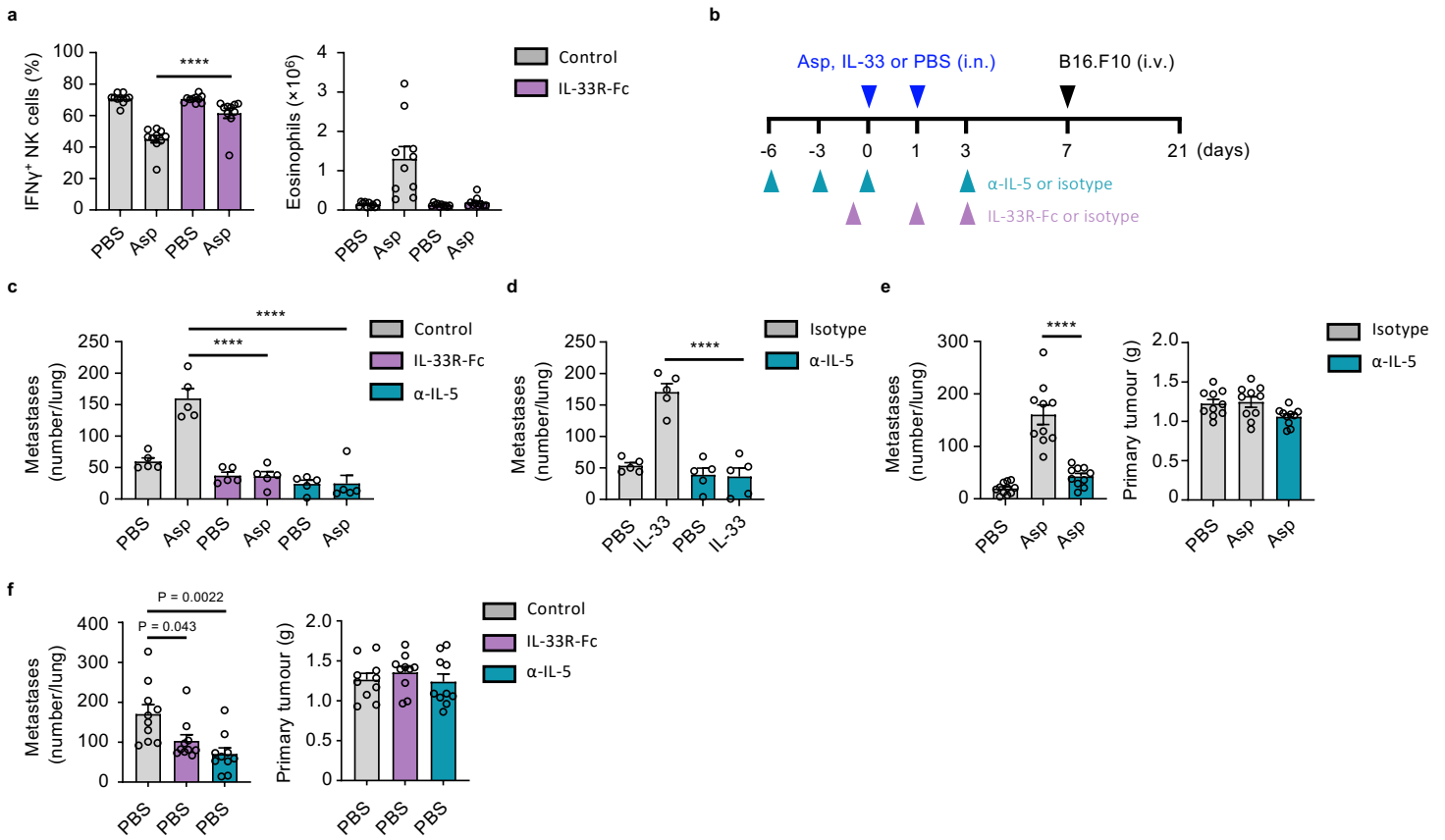


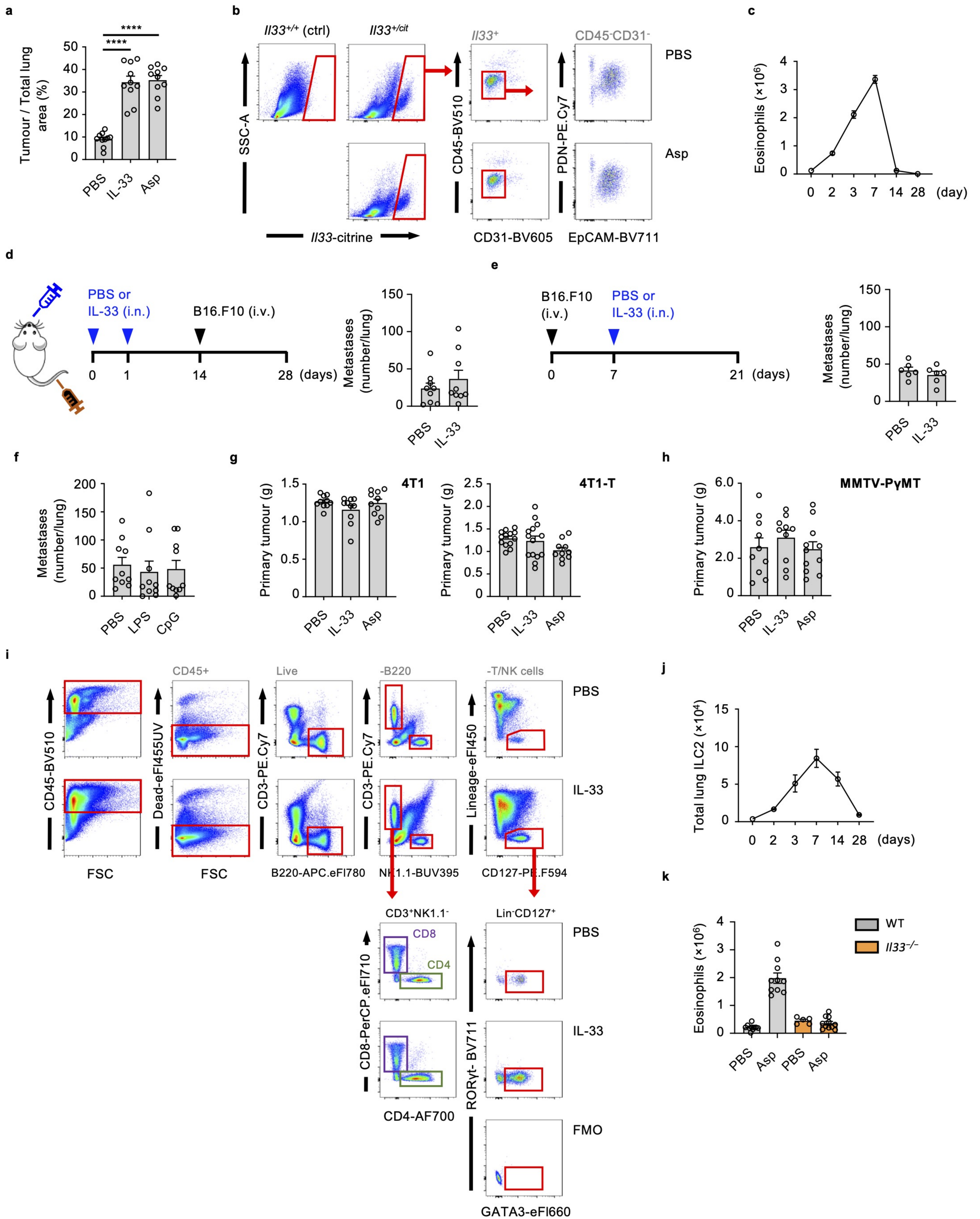


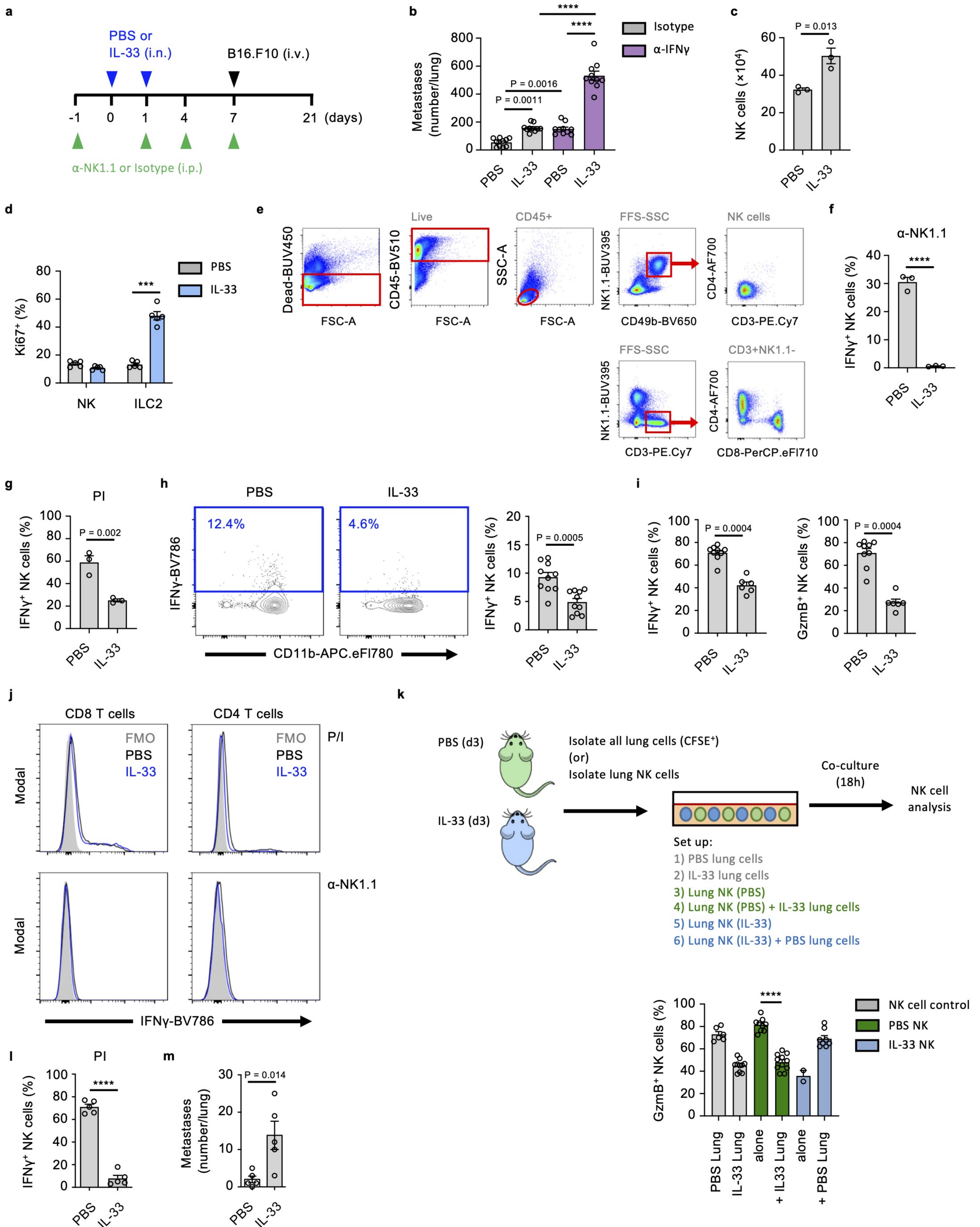


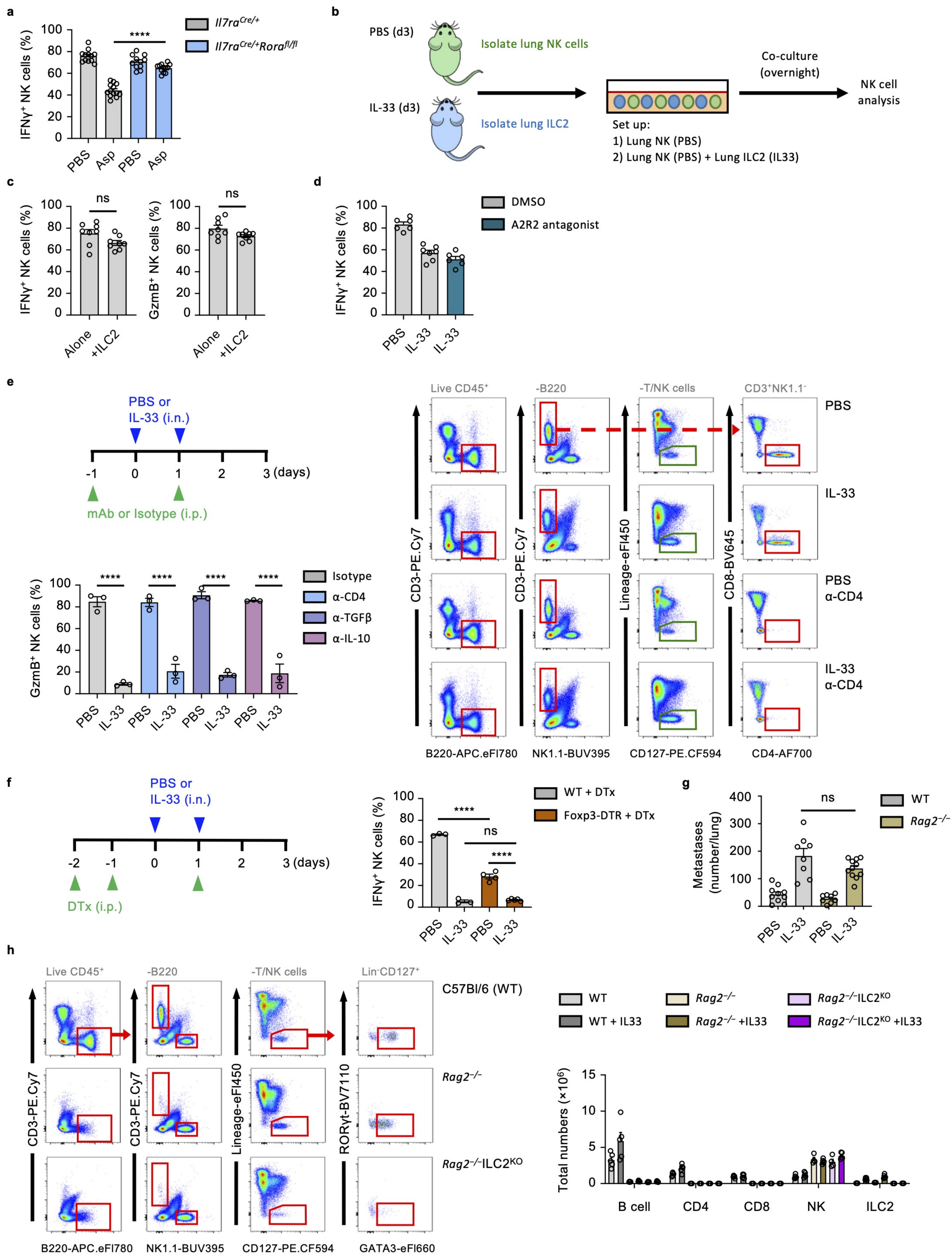


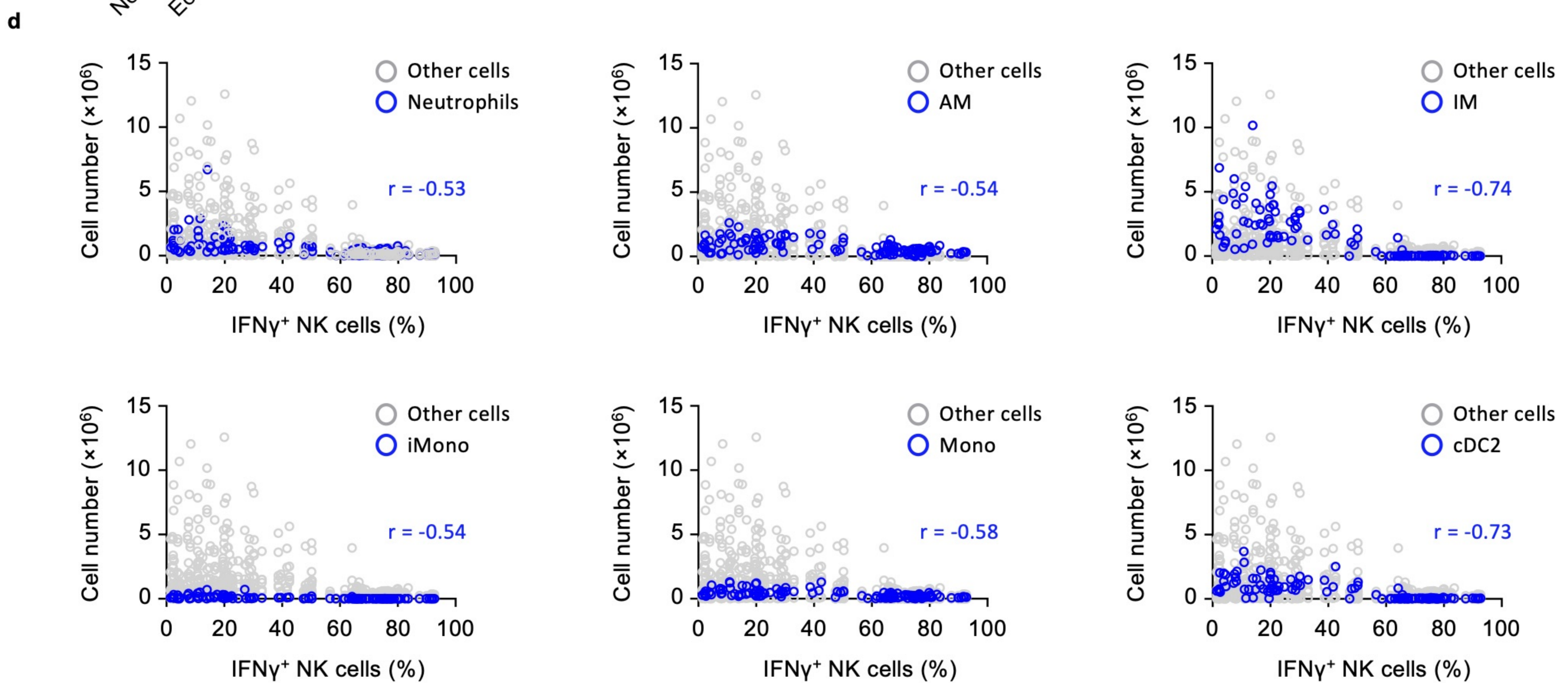
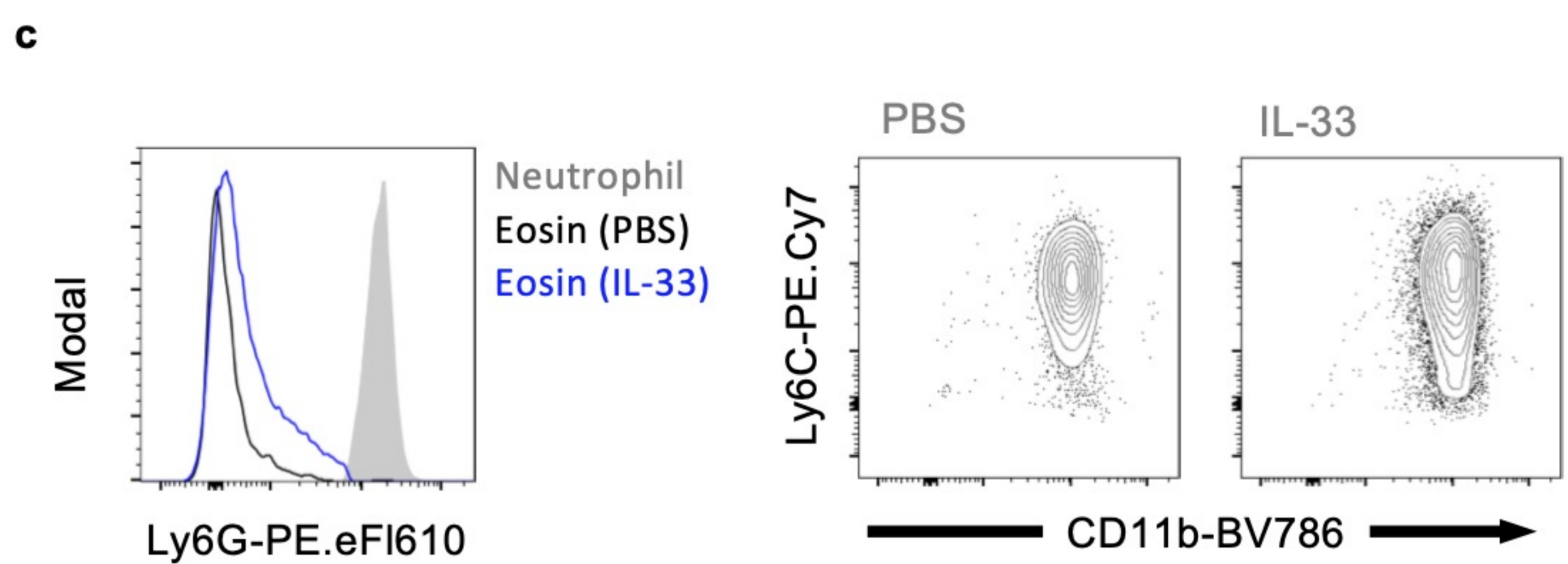
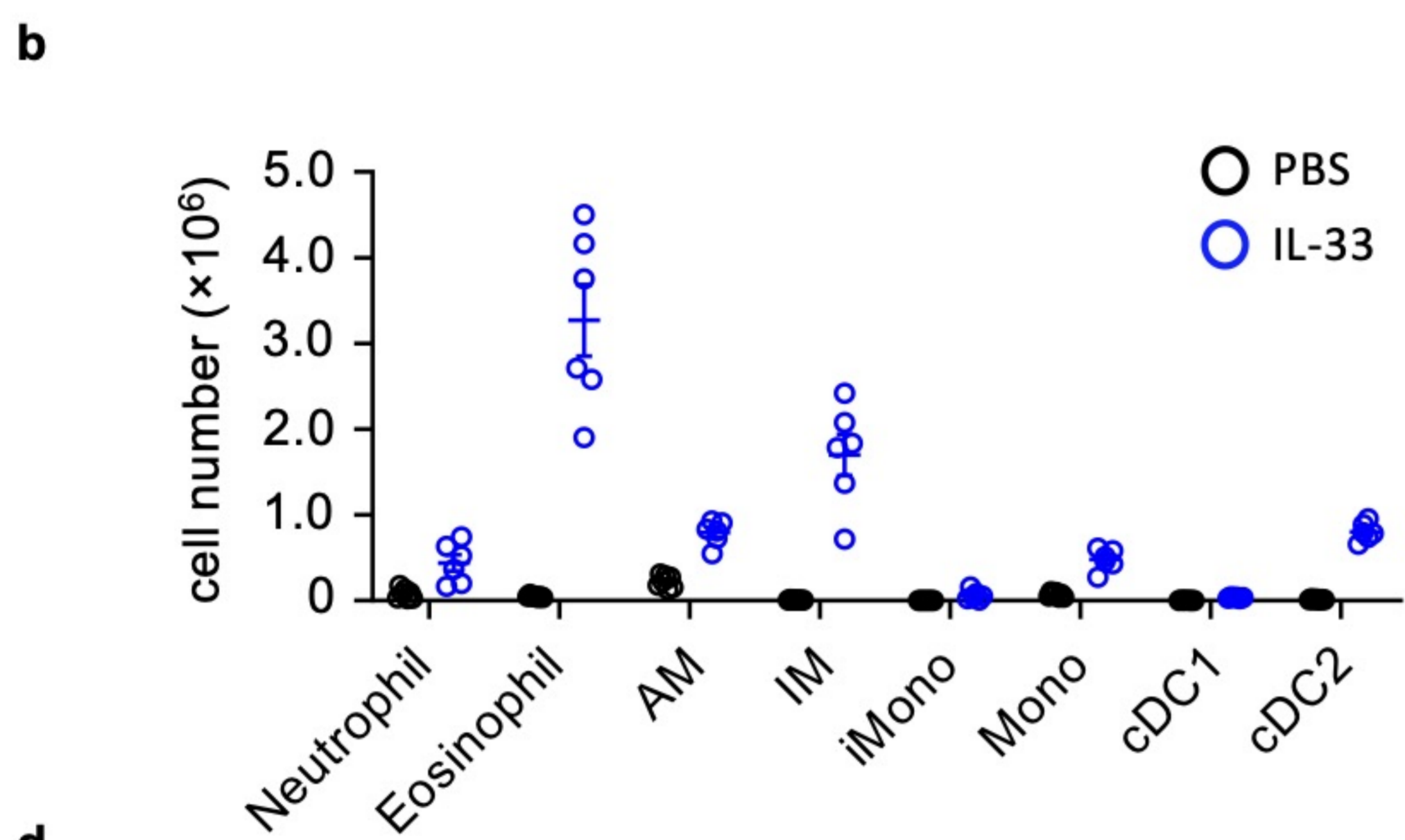
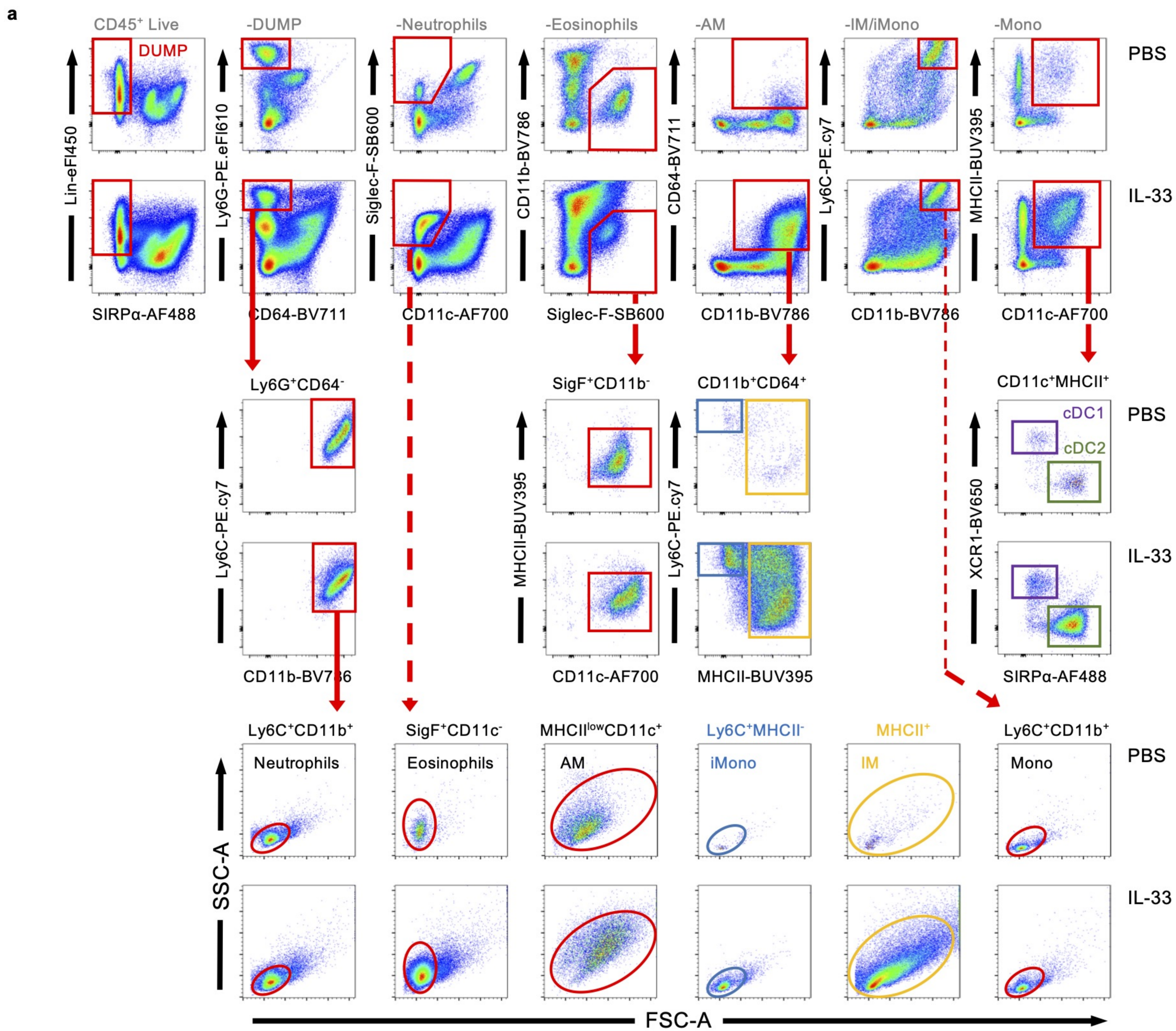


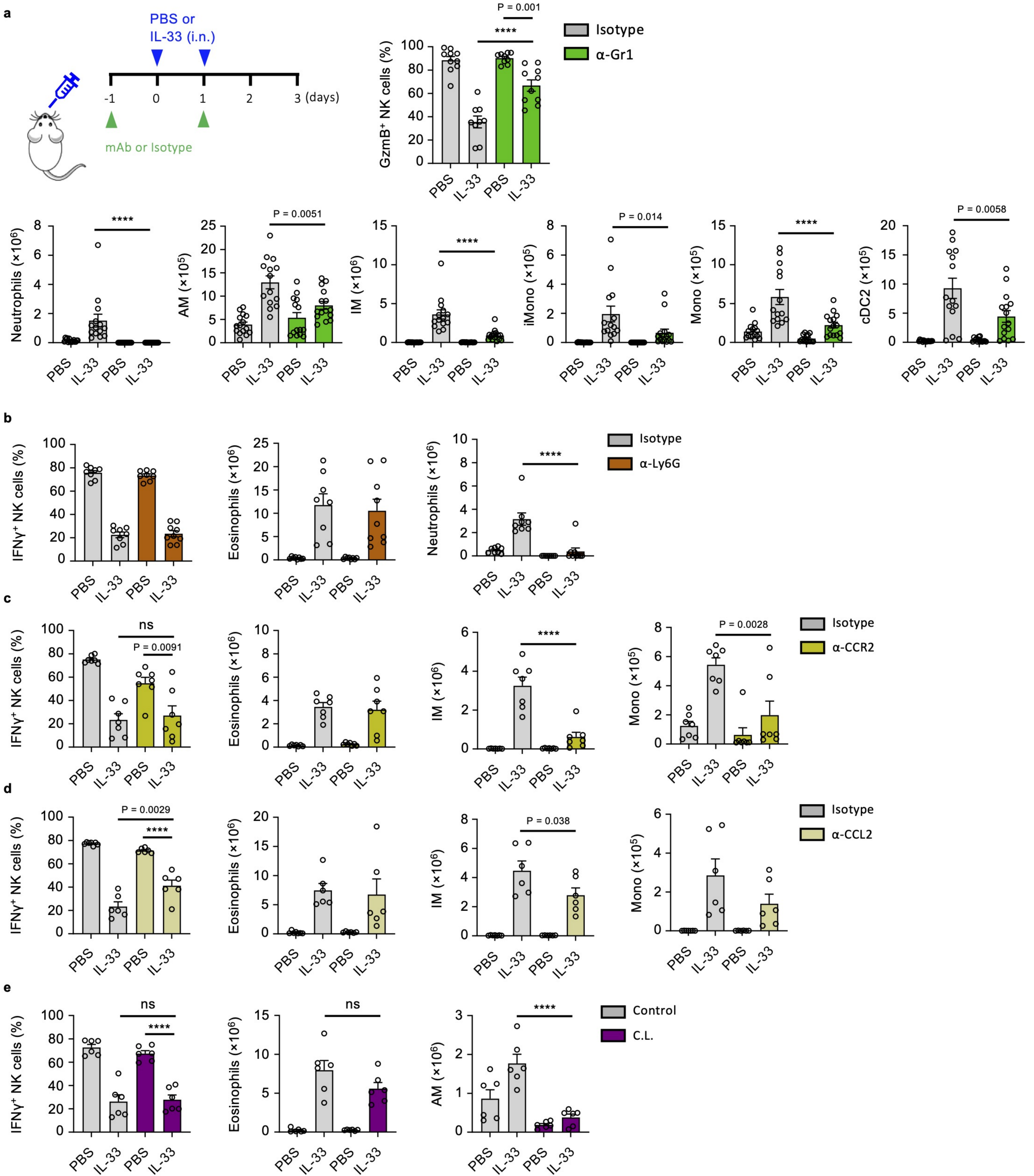


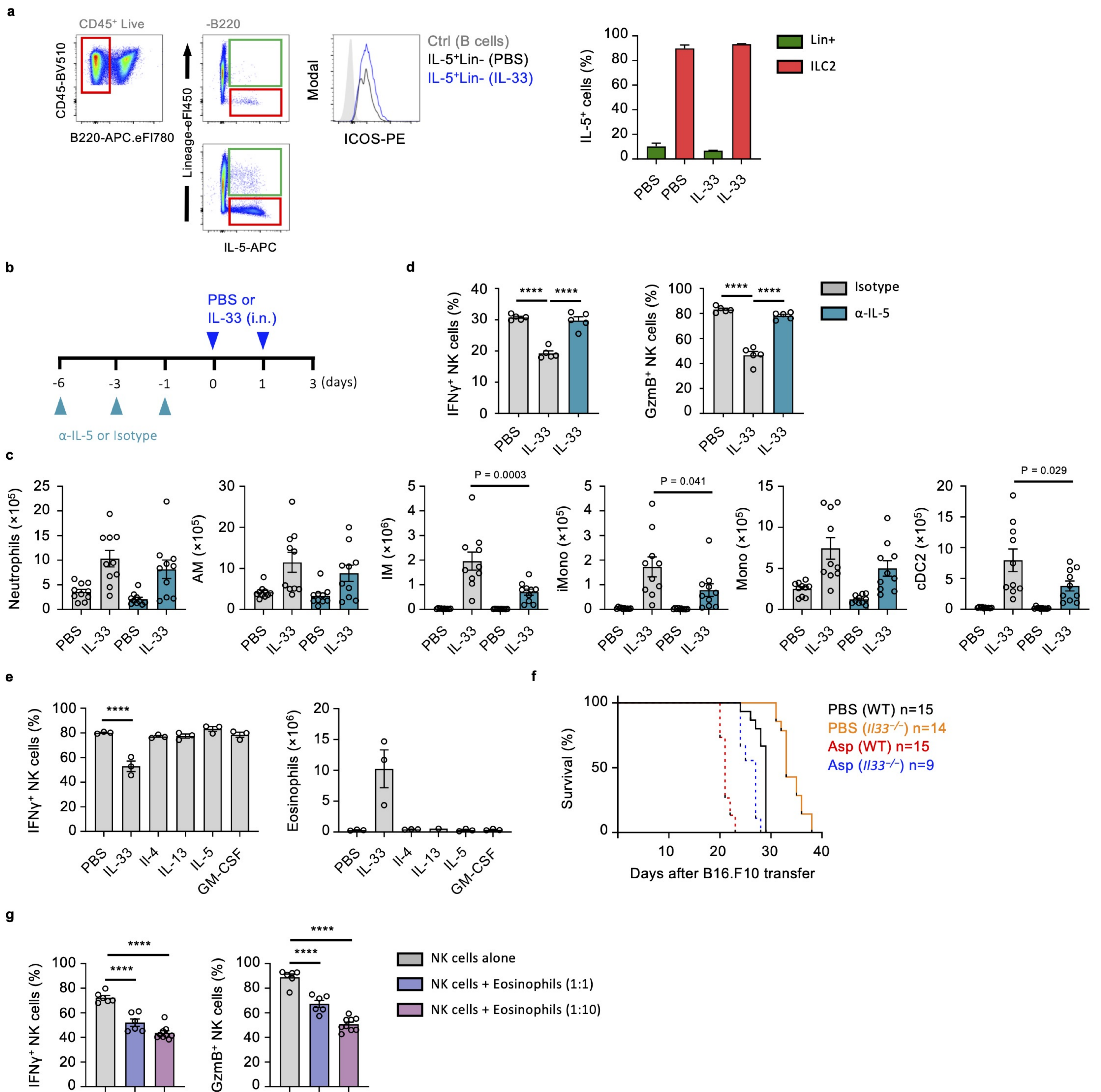


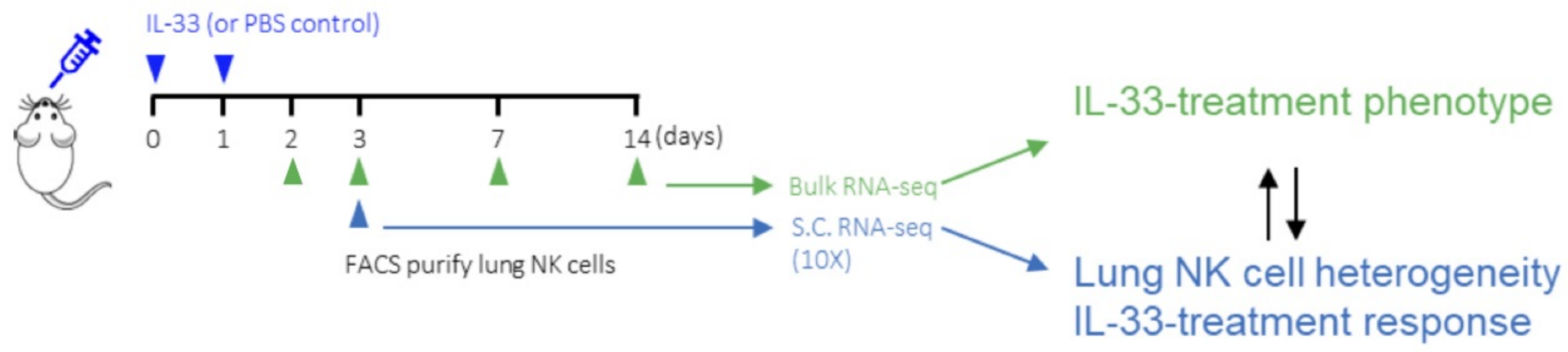
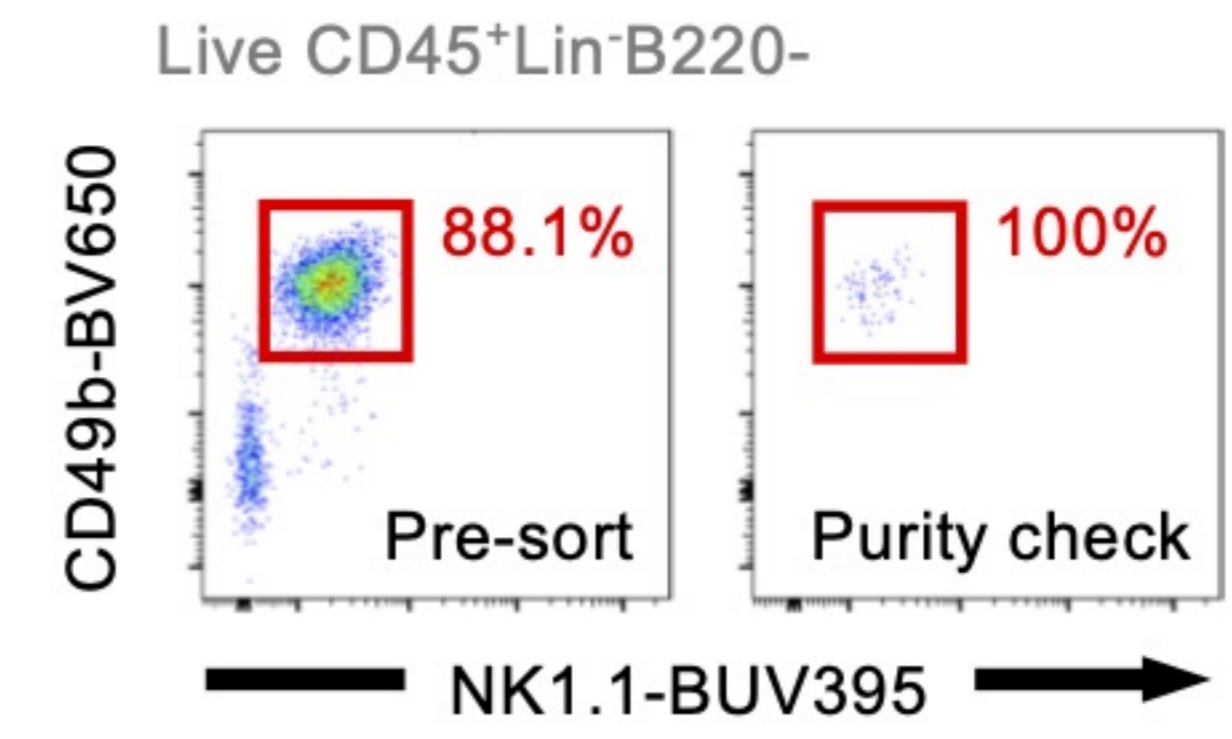
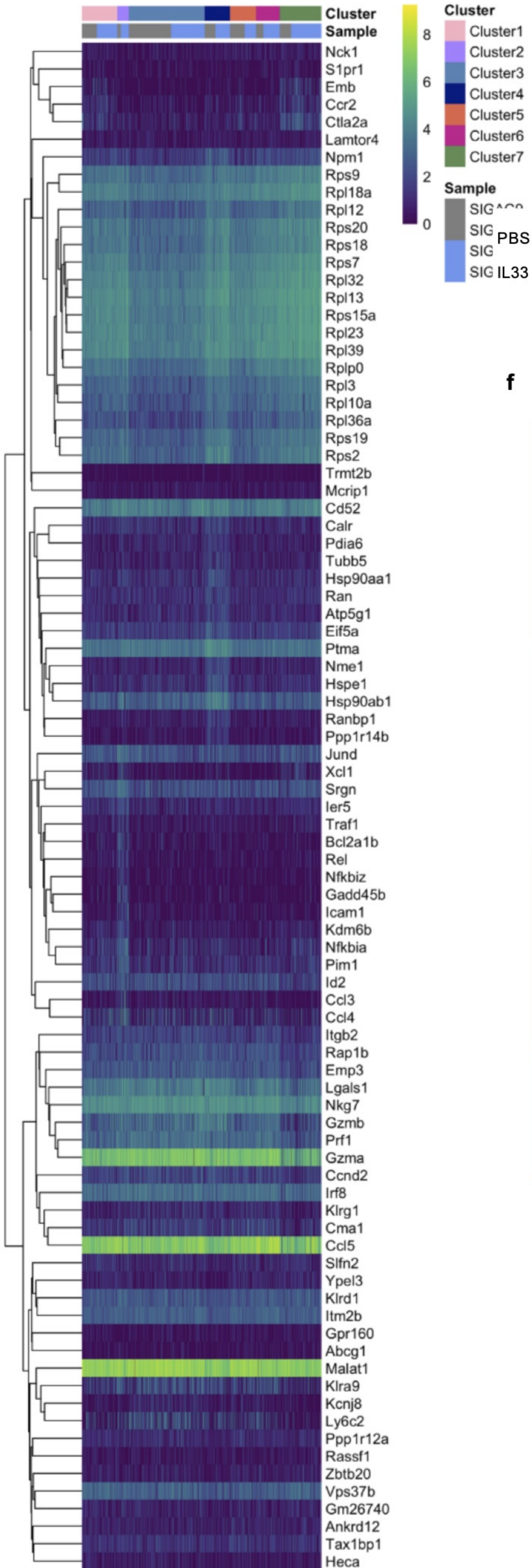
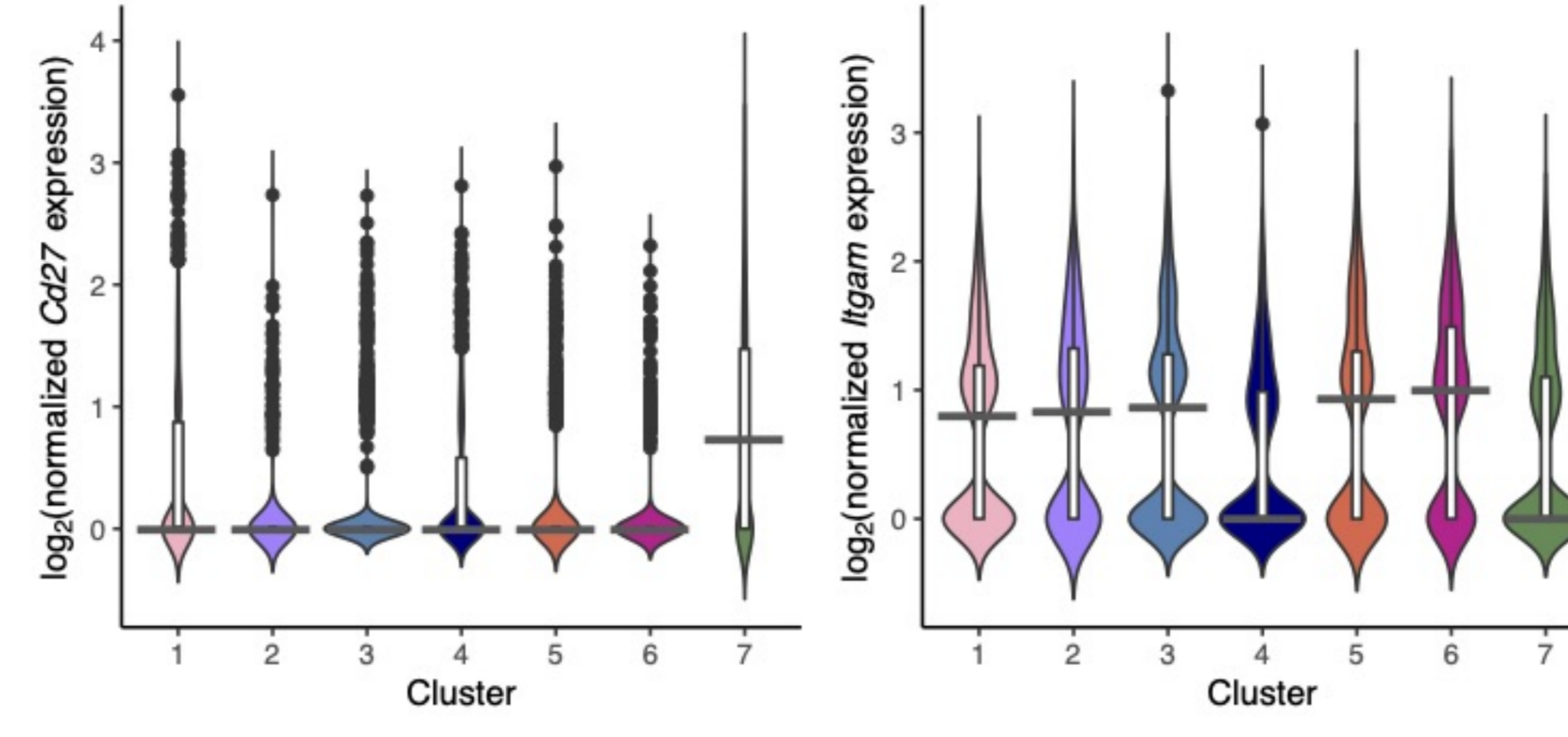




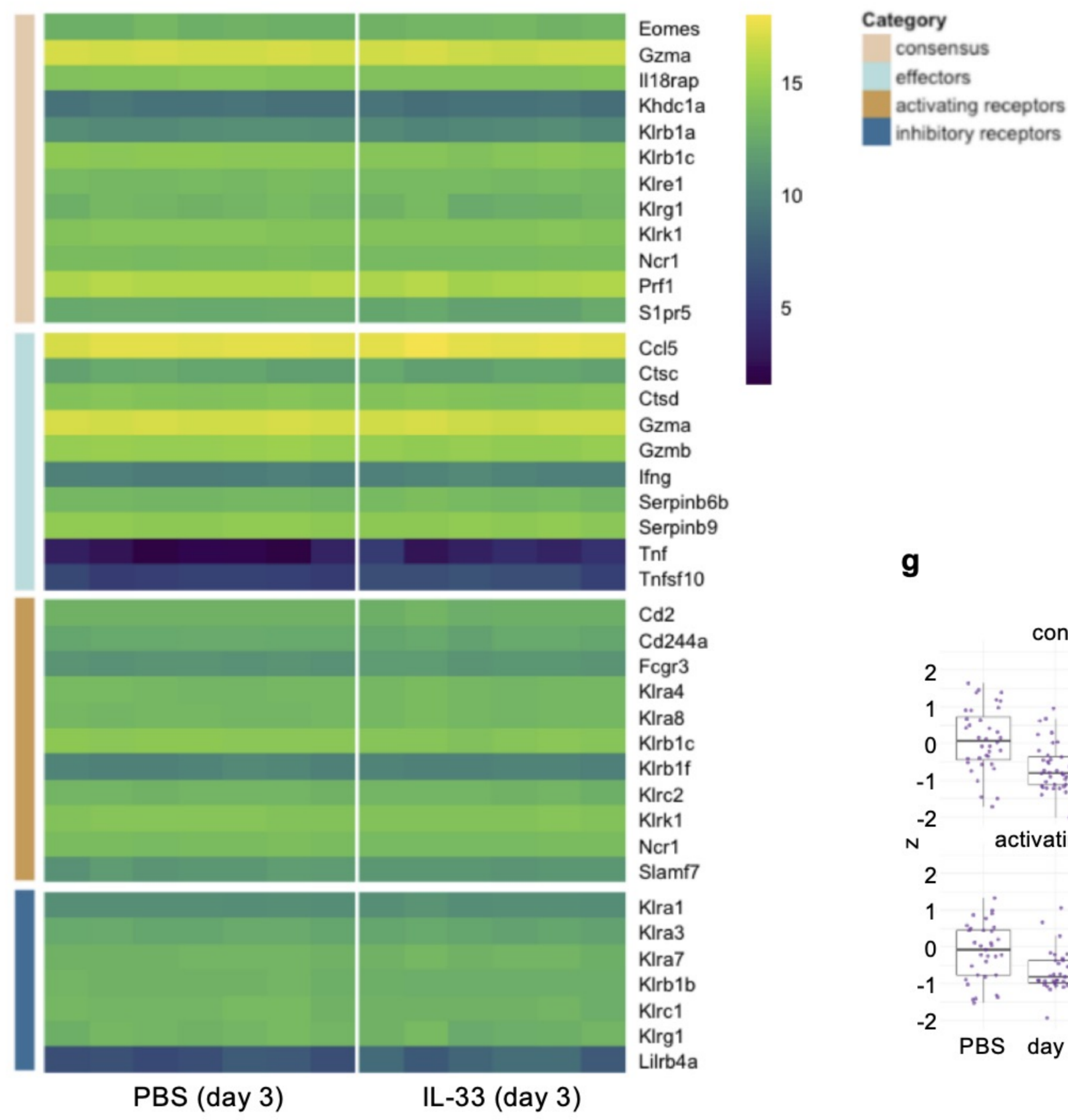






a**b****c****d****e**

Cluster	log ₂ (fold-change)	p-value	FDR
5	-0.731	0.003	0.013
7	1.010	0.004	0.013
2	0.740	0.007	0.013
3	-0.658	0.007	0.013
6	0.712	0.152	0.213
4	0.148	0.271	0.316
1	0.079	0.727	0.727

f**g**